COLLEGE OF ENGINEERING
NUCLEAR ENGINEERING & RADIOLOGICAL SCIENCES
UNIVERSITY OF MICHIGAN

Nuclear Reactor
Analysis & Methods
Group
NuRAM

NURAM-2020-004-00

Verification of MPACT for the APR1400 Benchmark

Kaitlyn Barr[1], Sooyoung Choi[1], and Brendan Kochunas[1]

[1] *University of Michigan*

11/06/2020

This page is intentionally blank.

REVISION LOG

Revision	Date	Affected Pages	Revision Description
0	11/06/2020	All	Initial Release

Document pages that are:

Export Controlled:	None
IP/Proprietary/NDA Controlled:	None
Sensitive Controlled:	None
Unlimited:	All

EXECUTIVE SUMMARY

This report describes several benchmark calculations performed using the transport code MPACT, that were compared to reference solutions generated by the Monte Carlo code McCARD in order to support continuous improvements to MPACT, increasing reliability of reactor modeling software, and test the capability of MPACT to model advanced reactors. The benchmarks are based on the Advanced Power Reactor 1400 MWe designed by the Korea Electric Power Corporation.

The reactor core is composed of 241 fuel assemblies. Nine assembly types are specified utilizing different configurations of 1.71 wt% UO_2, 2.00 wt% UO_2, 2.64 wt% UO_2, 3.14 wt% UO_2, 3.64 wt% UO_2, and gadolinia burnable absorbers. The reactor is controlled by seven control rod assembly banks. The banks are either 4-fingered or 12-fingered. The benchmark problems completed include single fuel pin, single 2-D fuel assembly, 2-D core, 3-D core, control rod worth, and 3-D core depletion. Nine temperature and boron conditions were considered for the various geometries. Additionally, MOC and spatial mesh parametric studies were performed using single fuel pins and single 2-D fuel assemblies to determine if default meshing parameters were sufficiently accurate.

For the calculations in this report, the MPACT 51-group cross section library based on ENDF-B/VII.1 was used. The calculations are performed with P_2 scattering. For the MOC discretization, the Chebyshev-Yamamoto quadrature type was used with a ray spacing of 0.05 cm, 16 azimuthal angles per octant, and 2 polar angles per octant.

Overall, MPACT shows excellent agreement compared to the Monte Carlo reference solutions generated by McCARD. MPACT effectively predicts the reactivity for different geometries as well as several temperature and boron conditions. The largest deviation from McCARD occurs for cold zero conditions in which the fuel, moderator, and cladding are all 300 K. This is likely due to an incorrect hydrogen scattering matrix used by MPACT. Excluding these cases, the ρ reactivity difference from McCARD is consistently below 100 pcm. For single fuel pin problems, the highest error occurs for the lowest fuel enrichment of 1.71 wt% UO_2, indicating possible, albeit small, enrichment bias in MPACT's cross section library. Furthermore, MOC and spatial mesh parametric studies indicate that default meshing parameters and options yield results comparable to finely meshed cases, thus verifying that default MOC and spatial discretization parameters generate accurate results for the benchmark problems.

Additionally, there is very good agreement of the radial and axial power distributions. Using P_2 scattering instead of the default TCP_0 scattering method corrected an in-out radial power tilt for the 2-D core, 3-D core, control rod worth, and 3-D core depletion problems. With P_2 scattering, the RMS pin and assembly power differences for all cases are below 1%, and all RMS axial power differences are below 1.65%. These results are comparable to previous results from the VERA progression problems benchmark.

Regarding the hot full power 3-D core depletion, there was some variation in the critical boron concentration calculated by MPACT compared to nTracer and DeCART. Future work entails investigating the reasons for these differences.

This page is intentionally blank.

CONTENTS

LIST OF FIGURES

LIST OF TABLES

ACRONYMS

ANL Argonne National Laboratory

CASL Consortium for the Advanced Simulation of Light Water Reactors

I-NERI International Nuclear Energy Research Initiative

KAERI Korea Atomic Energy Research Institute

MOC Method oc Characteristics

MPACT Michigan PArallel Characteristics Transport

ORNL Oak Ridge National Laboratory

%RMS relative Root Mean Square

T/H thermal/hydraulic

1. INTRODUCTION

To address pressing challenges to nuclear power, the United States Office of Nuclear Energy supports projects that reduce costs, improve safety, and limit proliferation risk [1]. International collaborations are essential to this work, leading to the formation of programs such as the International Nuclear Energy Research Initiative (I-NERI), which is a joint venture between the United States and the Republic of Korea. A current I-NERI program specifically aims to improve high-fidelity, multi-physics simulation codes for advanced nuclear reactors. Under this collaboration, the APR1400 benchmark has been developed to facilitate code-to-code verification [2]. The benchmark reference solution was generated by the Monte Carlo code McCARD [3]. Hence, the purpose of this report is to describe and present the results of a series of benchmark calculations performed using the MPACT code [4] and discuss the extent of agreement with the McCARD reference solution.

The benchmark problems are based on the core design of the Korea Electric Power Corporation APR1400. The APR1400 core consists of 241 fuel assemblies in a rectangular lattice. Each fuel assembly is composed of 236 fuel or burnable absorber rods, 4 guide tubes, and 1 central tube arranged in a rectangular lattice. The guide tubes and central tubes are the size of four regular pin cells. Nine assembly types are specified utilizing different configurations of 1.71 wt% UO_2, 2.00 wt% UO_2, 2.64 wt% UO_2, 3.14 wt% UO_2, 3.64 wt% UO_2, and gadolinia burnable absorbers. The reactor is controlled using seven control rod banks: two shutdown banks labeled A and B and five regular banks labeled 1, 2, 3, 4, and 5. Banks A, B, 1, and some of bank 2 have 12-fingered control rod assemblies, and some of bank 2 as well as all of banks 3, 4, and 5 have 4-fingered control rod assemblies. More details summarizing the benchmark problems are included in the following section, and the complete core specifications can be found in reference [2].

The analysis of these benchmark problems have been completed by researchers at the Seoul National University Reactor Physics Laboratory using nTRACER and at the Korea Atomic Energy Research Institute (KAERI) using DeCART. DeCART is a "whole core neutron transport code capable of direct subpin level flux calculation at power generating conditions" [5]. nTRACER is a "high-fidelity multi-physics simulation code" for commercial PWRs and fast reactors that utilizes a "direct whole core calculation module and a sub-channel thermal/hydraulic (T/H) solver" [6]. Both DeCART and nTRACER accurately predict reactivity in various geometries and conditions, with ρ reactivity differences from McCARD below 100 pcm in almost every case and control rod worth differences below 1.0%. For both codes, the greatest reactivity differences occur for cold zero conditions in which the fuel, moderator, and cladding are 300 K. These results are similar to those obtained using MPACT.

Regarding the power distribution, nTRACER results initially exhibited a radial power tilt, and this was resolved by correcting the reflector cross sections for the large spatial dependency of the multigroup cross-sections for stainless steel. Once this was done, RMS radial power distribution errors between nTRACER and McCARD were all below 1.0% and RMS axial power distribution errors were below 1.7%. Radial power distribution errors were higher for DeCART; most RMS radial power distribution errors are below 1%, but there are several outliers, most of which are cases with cold zero power conditions. All RMS radial power distribution errors are below 2.27%. All RMS axial power differences from McCARD are below 2.25%. Excluding cases with cold zero conditions, all axial power differences are below 1.52% [7]. These results indicate that both

DeCART and nTRACER effectively predict reactivity and power distributions for the APR1400, but errors are most significant for cases using cold zero conditions.

The remainder of the report is outlined as follows. In Section 2, the reactor geometry, benchmark problems, and conditions studied are described in detail. In Section 3, modeling parameters used in the MPACT models as well as equations relevant for the analysis are included. In Section 4, all benchmark problem results as well as the results of spatial and MOC parametric mesh studies on single pin and 2-D single assembly cases are presented. Finally, sections 5 and 6 contain conclusions and future work.

2. BENCHMARK PROBLEMS

The benchmark involves six problem types: single fuel pin, single 2-D fuel assembly, 2-D core, 3-D core, control rod worth calculations, and a 3-D core depletion. Additionally, mesh sensitivity studies were performed on the single fuel pin and single 2-D fuel assembly problems.

For each benchmark problem, several operating conditions are specified. For this report, cold zero (CZ) power refers to a moderator, cladding, and fuel temperature of 300 K. Hot zero (HZ) power indicates a moderator, cladding, and fuel temperature of 600 K. Hot full (HF) power refers to a moderator and cladding temperature of 600 K and a fuel temperature of 900 K. The specified boron concentrations are 0 ppm, 1000 ppm, and 2000 ppm. The naming convention adopted for describing benchmark results in this report references cases using two letters, that refer to the temperature condition, followed by a number, that indicates the boron concentration. A boron concentration of 0 ppm is indicated by a 0, 1000 ppm is indicated by a 1, and 2000 ppm is indicated by a 2. For example, when the moderator, fuel, and cladding temperature are all 300 K and the boron concentration is 1000 ppm, the case is referred to as CZ1. Table 1 summarizes the naming conventions for all temperature and boron conditions that are analyzed.

Table 1. Naming Convention for Various Temperature Conditions and Boron Concentrations.

Boron Concentration [ppm]	Temperature Conditions		
	CZP Fuel: 300 K Mod: 300 K	HZP Fuel: 600 K Mod: 600 K	HFP Fuel: 900 K Mod: 600 K
0	CZ0	HZ0	HF0
1000	CZ1	HZ1	HF1
2000	CZ2	HZ2	HF2

Fig. 1 - Fig. 7 show key elements of the APR1400 core configuration.

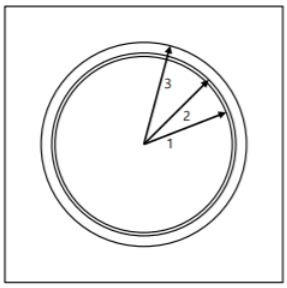

Region #	Size [cm]	Material
1	0.409575	UO2 Fuel
2	0.41873	AIR
3	0.47498	ZIRLO

Figure 1. Radial Configuration of Fuel Rod [2].

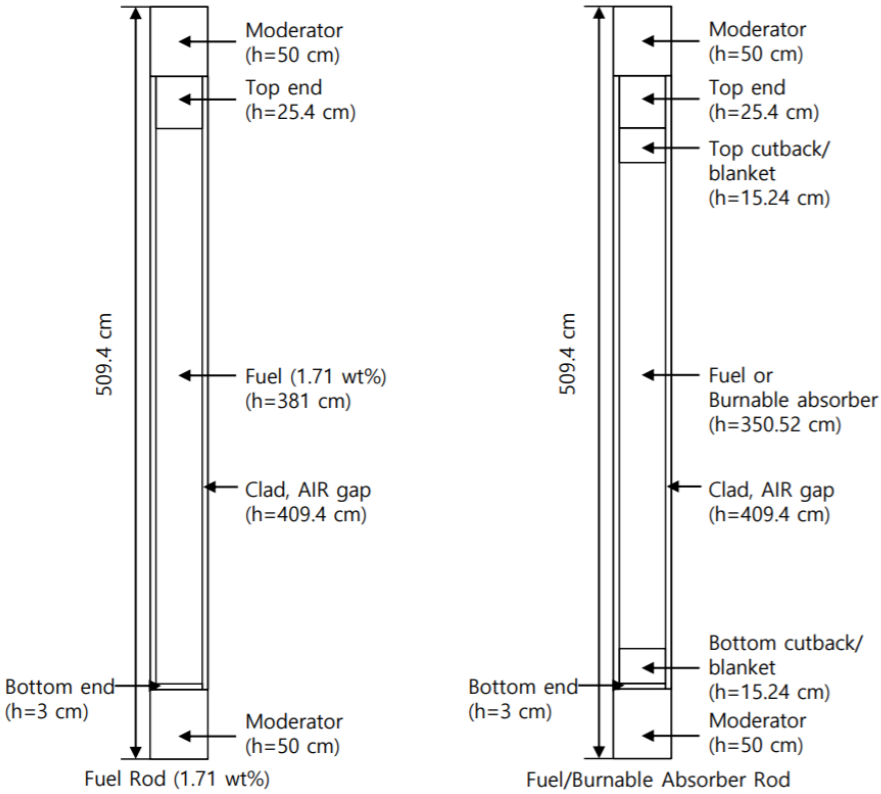

Figure 2. Axial Layout of Fuel and Burnable Absorber Rods in A0 Fuel Assembly (Left) and All Other Fuel Assemblies (Right) [2].

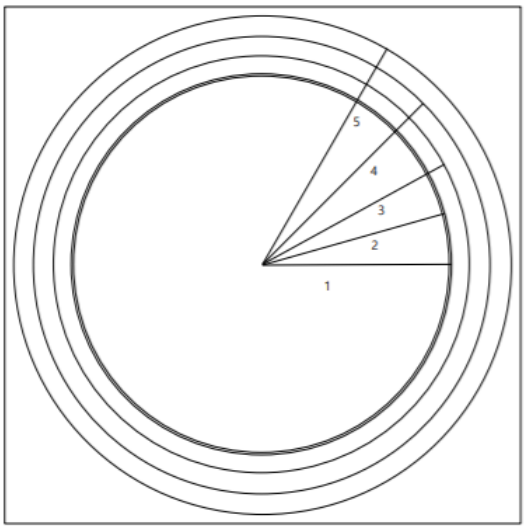

Region #	Size [cm]	Material
1	0.93599	B4C
2	0.94742	AIR
3	1.03632	INC625
4	1.13764	MOD
5	1.23	ZIRLO

Figure 3. Radial Configuration of Guide Tube with Control Rod Insertion [2].

All guide tubes and central tubes are the same size as four pin cells, which can be seen in Fig. 4, which depicts the radial configuration of a fuel assembly.

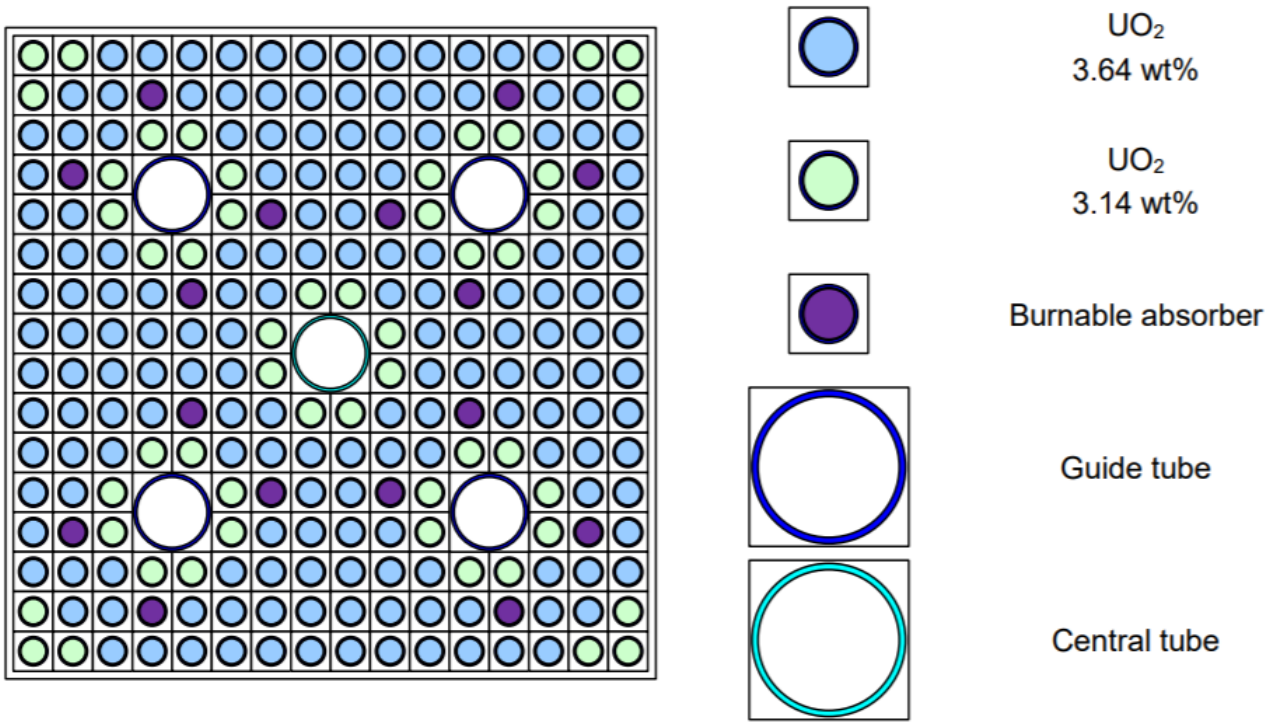

Figure 4. Radial Layout of C2 Fuel Assembly [2].

Each assembly has nine spacer grids with the axial layout shown in Fig. 5.

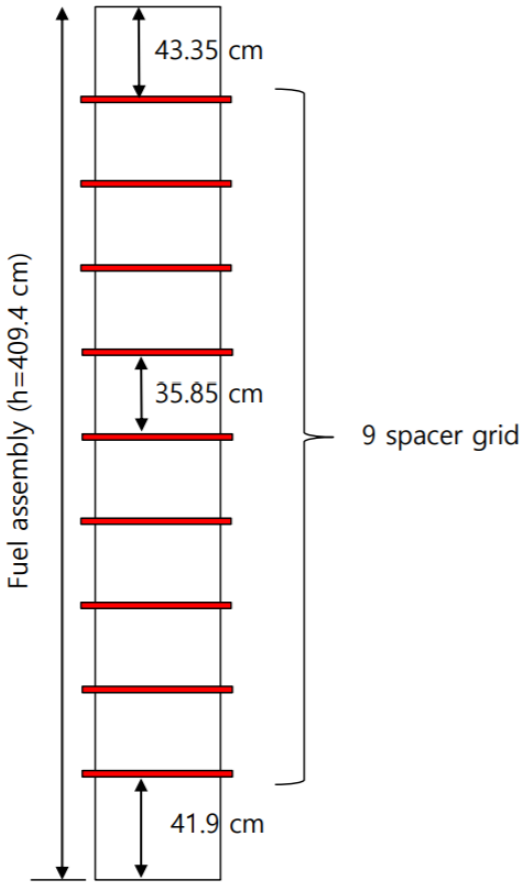

Figure 5. Axial Layout of Fuel Assembly Spacer Grids [2].

Nine assembly types are specified using five different fuel enrichments (1.71 wt% UO_2, 2.00 wt% UO_2, 2.64 wt% UO_2, 3.14 wt% UO_2, and 3.64 wt% UO_2) and gadolinia burnable absorbers. The core layout is shown in Fig. 6.

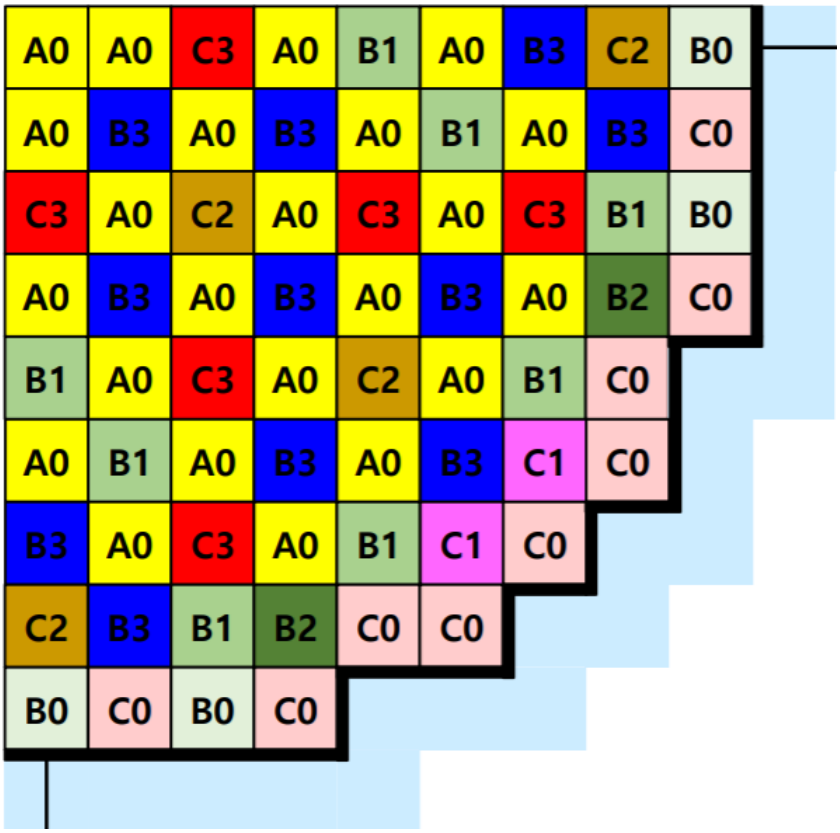

Figure 6. APR1400 Core Loading Pattern [2].

The reactor is controlled by seven control rod banks: five regulating banks, labeled 1, 2, 3, 4, and 5, and two shutdown banks, labeled A and B, as shown in Fig. 7. Banks A, B, 1, and some of bank 2 2 are composed of 12-fingered control rod assemblies, and the rest of bank 2 as well as banks 3, 4, and 5 are composed of 4-fingered control rod assemblies.

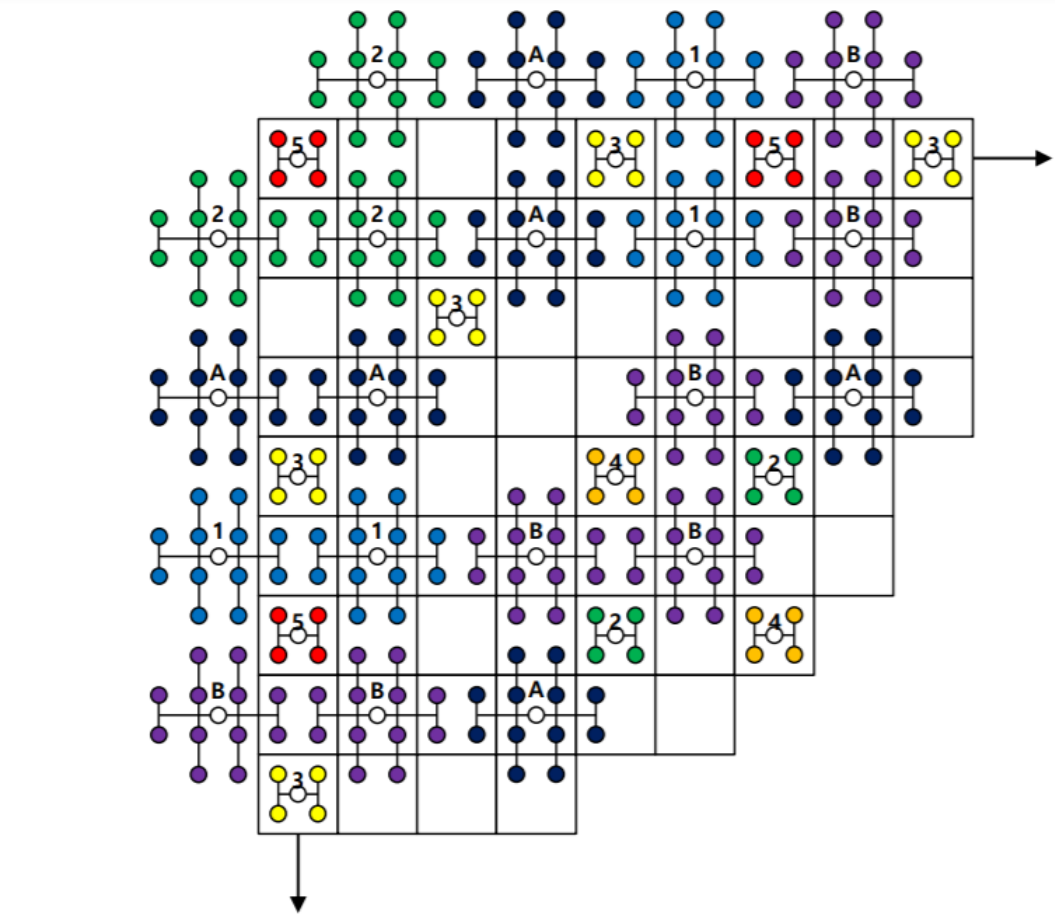

Figure 7. Control Rod Assembly Configuration [2].

Fig. 8 through Fig. 18 depict the single fuel pin, single 2-D fuel assembly, and 2-D core problem geometries as modeled in MPACT. The light blue background represents water as the coolant and moderator, light grey is cladding, purple is gadolinia burnable absorbers, and different fuel enrichments are represented by a spectrum ranging from dark blue, representing the lowest enrichment of 1.71 wt% UO_2, to maize, representing the highest enrichment of 3.64 wt% UO_2.

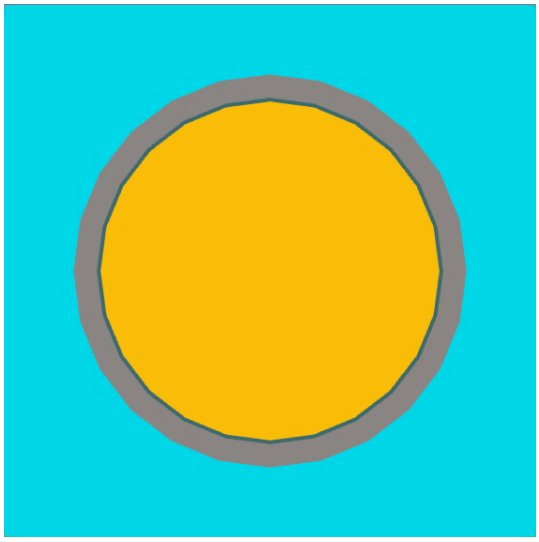

Figure 8. Single Fuel Pin Cell with 3.64 wt% UO_2 as Modeled by MPACT.

There are nine different fuel assemblies: A0, B0, B1, B2, B3, C0, C1, C2, C3. They utilize different configurations of 1.71 wt% UO_2, 2.64 wt% UO_2, 3.14 wt% UO_2, 3.64 wt% UO_2.

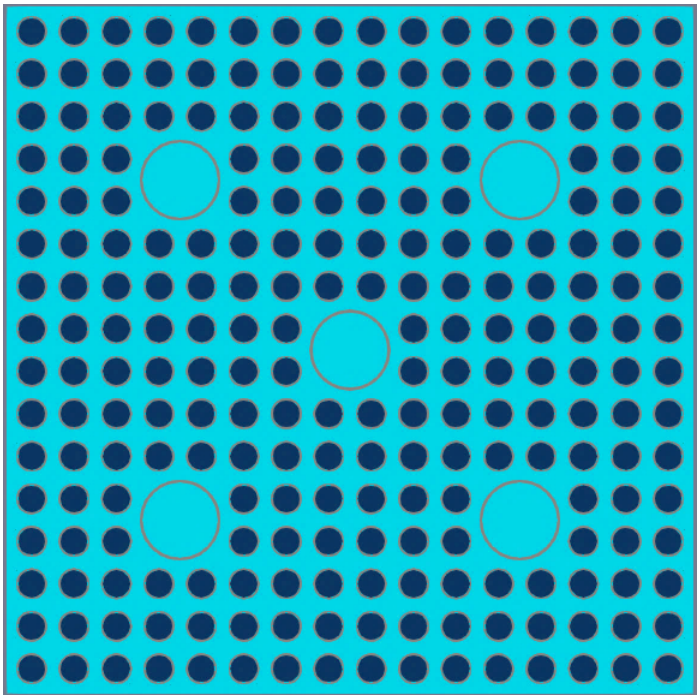

Figure 9. A0 Fuel Assembly Model Generated by MPACT.

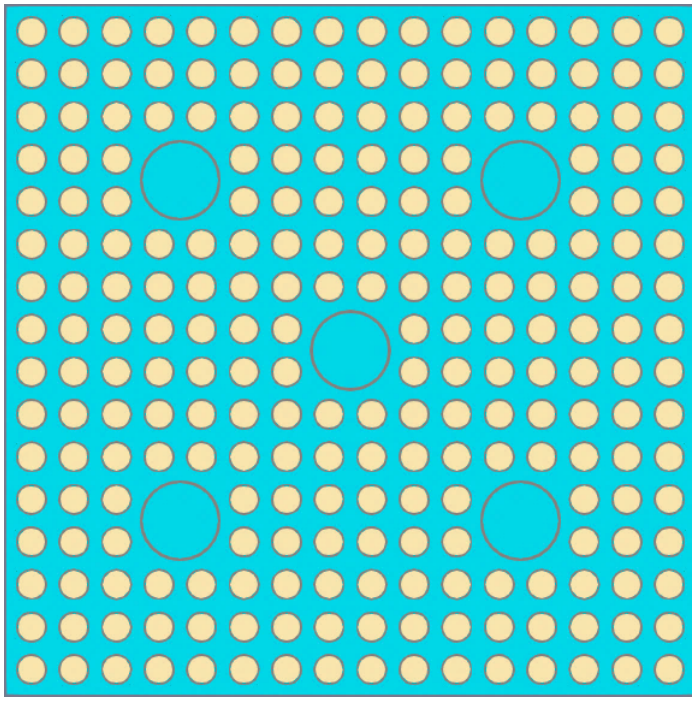

Figure 10. B0 Fuel Assembly Model Generated by MPACT.

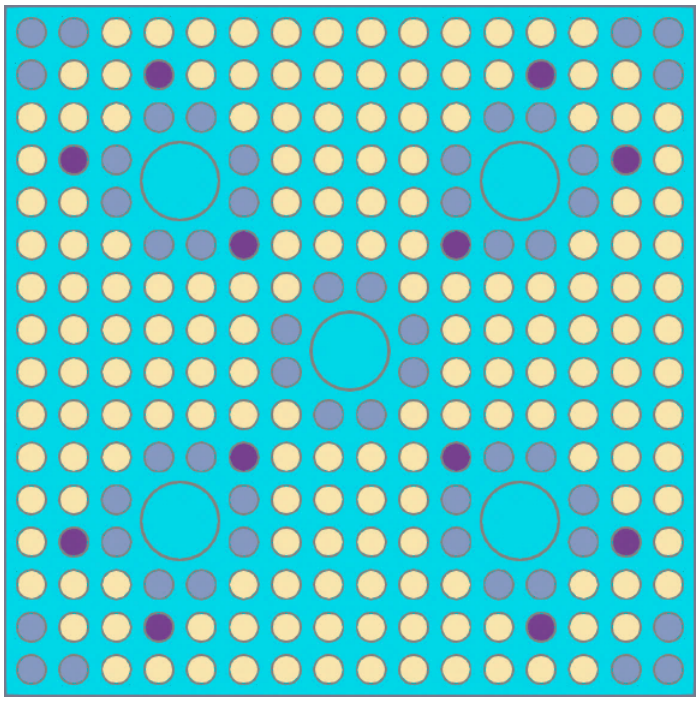

Figure 11. B1 Fuel Assembly Model Generated by MPACT.

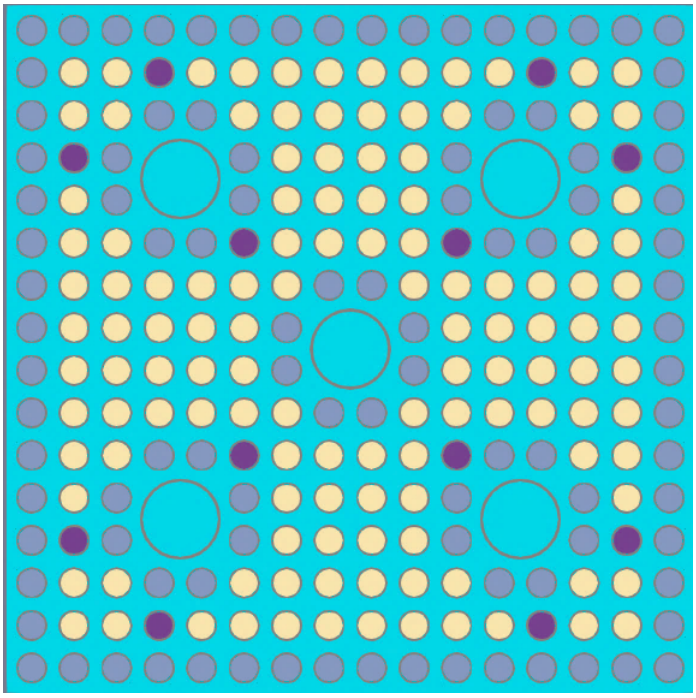

Figure 12. B2 Fuel Assembly Model Generated by MPACT.

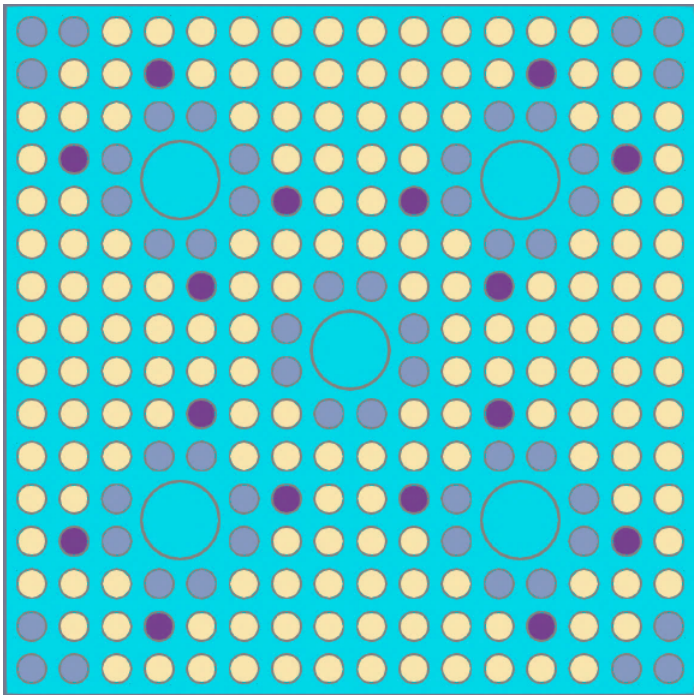

Figure 13. B3 Fuel Assembly Model Generated by MPACT.

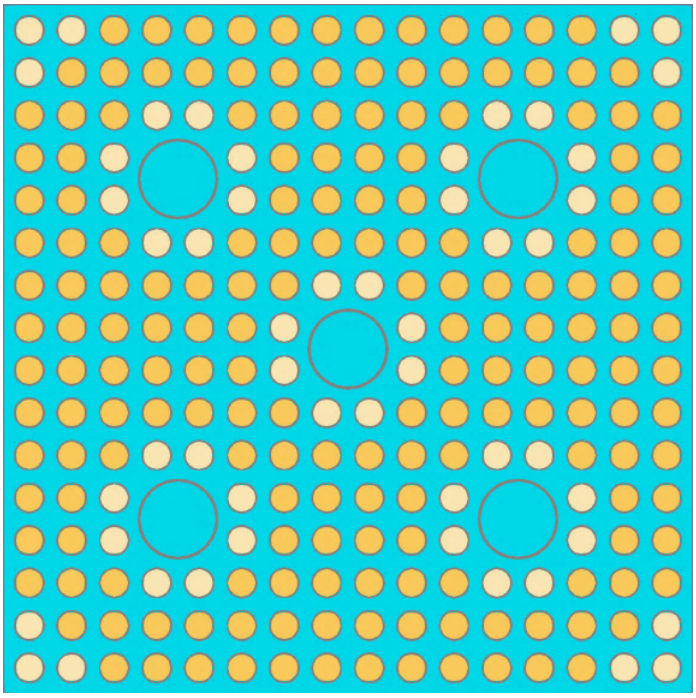

Figure 14. C0 Fuel Assembly Model Generated by MPACT.

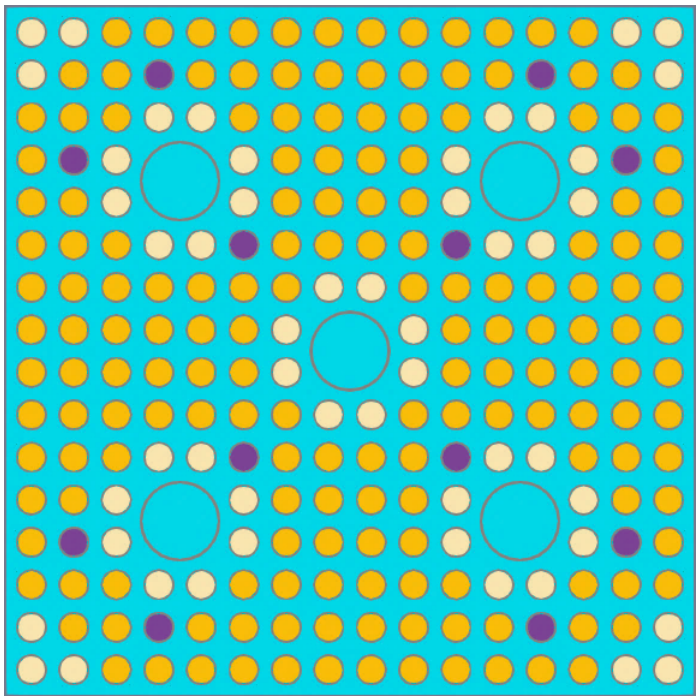

Figure 15. C1 Fuel Assembly Model Generated by MPACT.

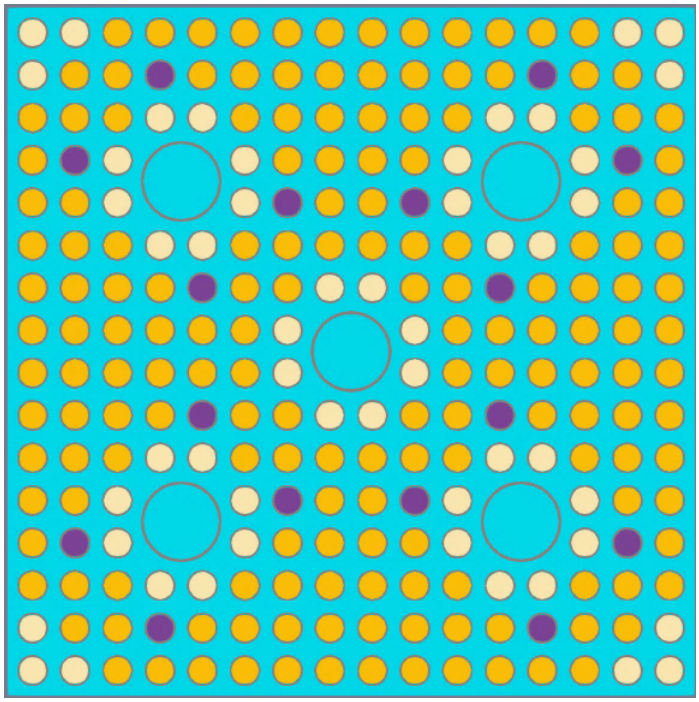

Figure 16. C2 Fuel Assembly Model Generated by MPACT.

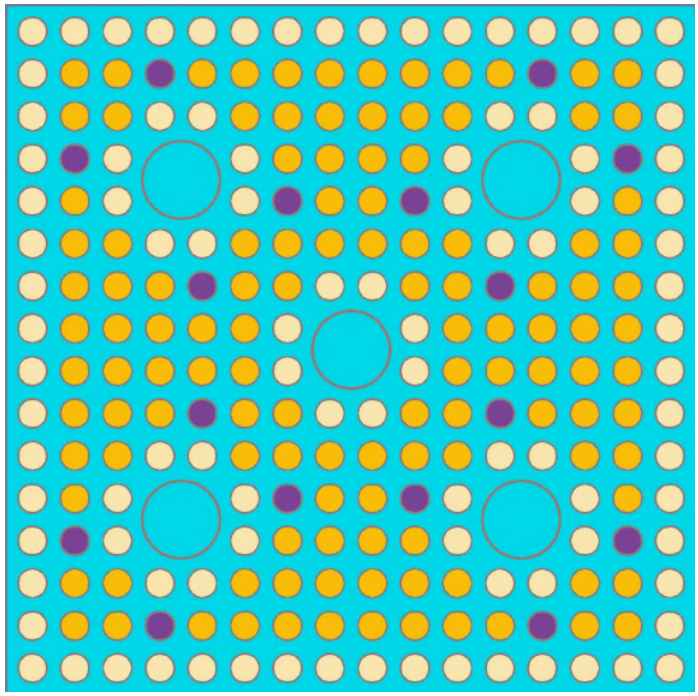

Figure 17. C3 Fuel Assembly Model Generated by MPACT.

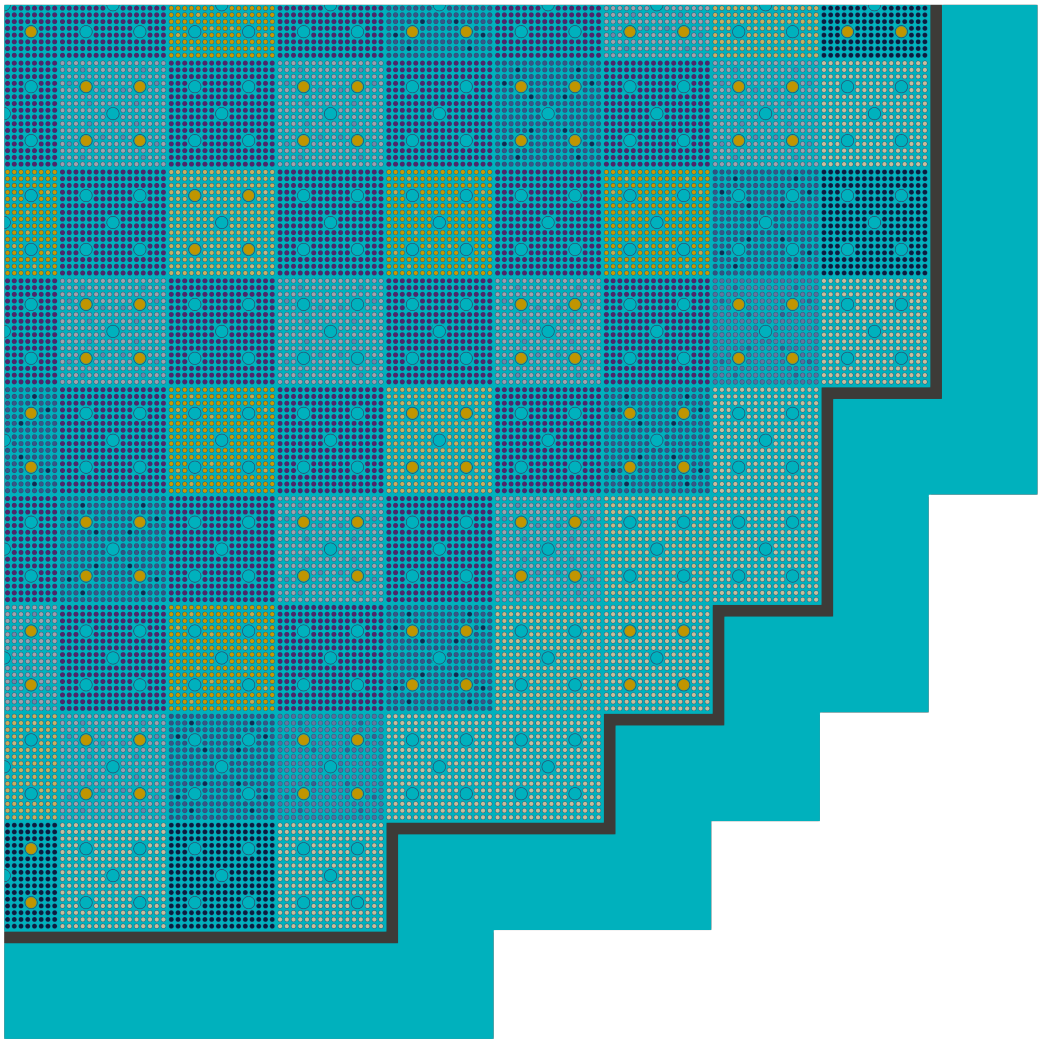

Figure 18. 2D Core Model Generated by MPACT.

3. METHODOLOGY

3.1 Modeling Parameters

Results were generated using MPACT's 2-D transport solver. All cases used the `mpact51g_71_4.3m2_03262018` 51-group cross-section library and default meshing parameters. For pin cells, the default Method oc Characteristics (MOC) flat source discretization was used. In fuel cells, the default flat source discretization creates 3 equal-area radial subdivisions in the fuel and one ring each in the fuel-clad gap, zircaloy cladding, and moderator. The guide tube pin cell has 3 radial subdivisions in the interior moderator and radial subdivision each in the cladding and external moderator. In the gadolinia burnable absorbers, there are 10 radial subdivisions in the fuel and 1 radial subdivision in all other regions. Each radial subdivision in all cell types has 8 azimuthal divisions. The flat source characteristics solver was used instead of the linear source

characteristics solver because the linear source solver is still undergoing validation. For the MOC discretization, the Chebyshev-Yamamoto quadrature type was used with a ray spacing of 0.05 cm, 16 azimuthal angles per octant, and 2 polar angles per octant. The P_2 scattering method was used for all problems.

All materials were defined based on the isotope number densities provided in the benchmark specifications [2]. However, there were some isotopes missing from MPACT's cross section library for which substitutions were necessary. Specifically, for silicon, carbon, and molybdenum, the benchmark specified number densities for individual stable isotopes of these elements, but MPACT's cross-section library does not have entries for the individual isotopes. Rather, the cross sections for natural silicon, natural carbon, and natural molybdenum were used instead because the number densities of various isotopes in the natural elements are the same as the individual isotopes specified in the benchmark.

3.2 Relevant Equations for Analysis

3.2.1 Reactivity differences

All reactivity differences are reported in terms of $\Delta\rho$, where $\Delta\rho$ is defined in Eq. (1).

$$\Delta\rho = \frac{1}{k_{McCARD}} - \frac{1}{k_{MPACT}}. \tag{1}$$

When results from multiple cases are combined, the arithmetic mean of $\Delta\rho$ is used.

3.2.2 Pin and assembly power comparisons

Pin and assembly power comparisons are usually reported in terms of the relative Root Mean Square (%RMS) difference. The relative difference, ϵ, between MPACT and McCARD is defined in Eq. (2).

$$\epsilon = \frac{Power_{MPACT} - Power_{McCARD}}{Power_{McCARD}}. \tag{2}$$

Using this result, the %RMS different is defined in Eq. (3).

$$\%RMS = \sqrt{\frac{\sum_{i=1}^{n} (\epsilon)_i^2}{n}} \tag{3}$$

where i is the pin or assembly index, and n is the total number of pins or assemblies considered. For maximum pin and assembly power differences, the relative maximum difference of all pins or assemblies considered, calculated using the above relative difference formula, is used.

4. RESULTS

4.1 Single Fuel Pin

4.1.1 Benchmark problem results

For the single pin problems, each of the five enrichments (1.71 wt% UO_2, 2.00 wt% UO_2, 2.64 wt% UO_2, 3.14 wt% UO_2, and 3.64 wt% UO_2) was modeled for each of the nine temperature and boron conditions, for a total of 45 cases studied. The complete isotopic compositions of the fuel are specified in the benchmark and were manually defined in the inputs. Fig. 19 is a histogram depicting the number of cases that fall in each reactivity difference range defined on the horizontal axis.

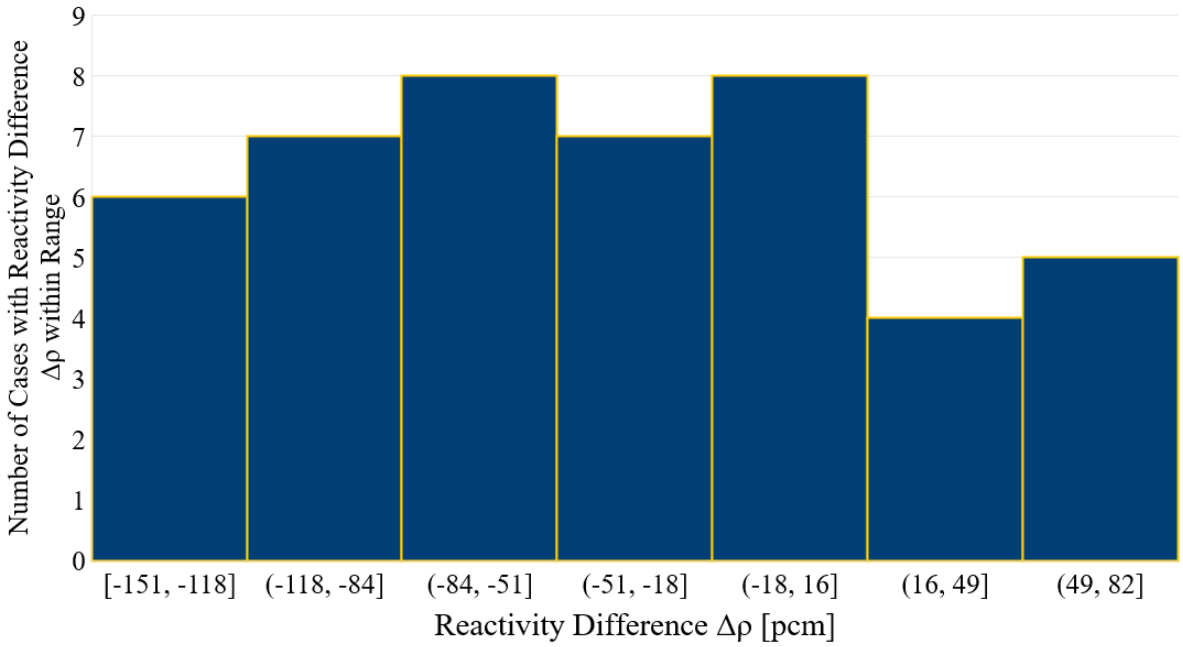

Figure 19. Histogram of Reactivity Differences for Single Fuel Pin Cases.

MPACT and McCARD generally agree very well; the average difference in kinf between the two solutions was 63 pcm ± 44 pcm, which can be attributed to MPACT's usage of a multigroup approximation as opposed to McCARD's continuous energy cross section representation. In 34 of the 45 cases studied, MPACT had a lower k_{inf} than McCARD, demonstrating a possible bias in the cross-section libraries. The maximum difference in k_{inf} was 151 pcm, and the minimum difference was 3 pcm.

Table 2 contains the average reactivity difference, standard deviation, and maximum reactivity difference for various categories of cases to better identify specific trends in the results. It was determined that the largest relative differences were observed for cases with an enrichment of 1.71 wt% UO_2, suggesting a possible, slight enrichment bias of approximately -50 pcm, although the exact value depends on other conditions, e.g. temperature, moderator density, boron concentration, in MPACT's cross section library. Additionally, boron concentration had a moderate impact on accuracy, as observed in Table 2, which shows agreement with McCARD generally improving as boron concentration increases.

Table 2. Average reactivity difference, standard deviation, and maximum difference for various groups of single fuel pin cases

Condition	Average k_{inf} $\Delta\rho$ [pcm]	Standard Deviation [pcm]	Maximum Difference [pcm]
Overall	63	44	151
0 ppm	110	22	151
1000 ppm	44	32	123
2000 ppm	28	35	82
1.71 wt%	79	76	151
2.00 wt%	66	73	134
2.64 wt%	58	67	122
3.00 wt%	53	61	116
3.64 wt%	48	57	104
CZ	75	87	151
HZ	64	47	104
HF	60	49	138

Reference [8] outlines several accuracy goals, including that reactivity differences should be below 200 pcm. Given that the maximum reactivity difference from McCARD for pin cell cases is 151 pcm, these results are acceptable.

4.1.2 MOC parametric studies

MOC parameters were individually altered for each of the 3.64 wt% enriched single pin cases, including all temperature and boron conditions, and compared to the k_{inf} generated by McCARD. Variations included using 4, 8, and 32 azimuthal angles per octant instead of the default 16; 1 and 3 polar angles per octant instead of the default 2; and 0.025 cm, 0.01 cm, and 0.005 cm ray spacing instead of the default 0.05 cm. Fig. 20 summarizes the average differences between the k_{inf} generated using each of these parameters and the k_{inf} generated by McCARD.

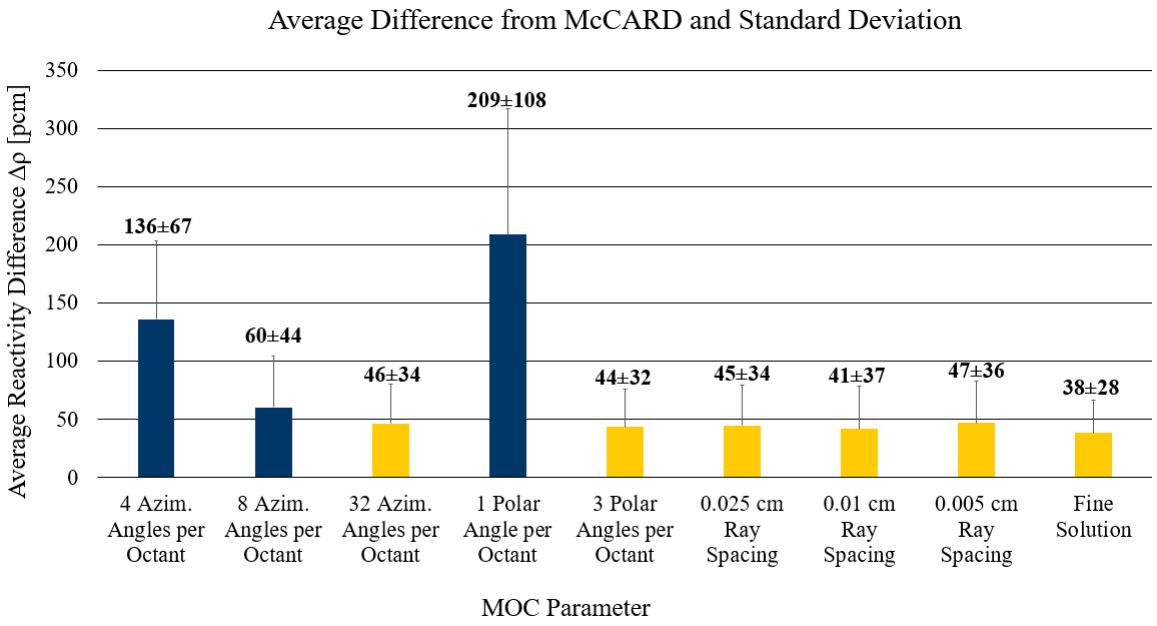

Figure 20. Average difference from McCARD k_{inf} and standard deviation for single pin MOC studies.

In Fig. 20, blue bars indicate parameters that are less fine than the default values, and maize bars indicate parameters that are finer than the default. Significant disagreement ranging from an average of 60 pcm to 209 pcm exists when parameters are made less fine than the default. The maximum absolute difference from McCARD is 369 pcm. On the other hand, making the MOC parameters finer reduces the average ρ difference from McCARD with errors ranging from 38 pcm to 47 pcm. Since the average difference from McCARD for pins with 3.64 wt% UO_2 using default values was 48 pcm, as stated in Table 2, there is a slight improvement in agreement with McCARD when using parameters finer than the default.

One of the parametric studies performed combined all the finest parameters and was called the "fine" solution. The fine solution had a ray spacing of 0.005 cm, 32 azimuthal angles per octant, and 3 polar angles per octant. The error from the McCARD k_{inf} for the fine solution is only 38 pcm, which is 10 pcm lower than the error when using default parameters. Fig. 21 and Fig. 22 are histograms the number of cases that fall in each reactivity difference range defined on the horizontal axis for the fine solution (Fig. 21) and when default parameters are used (Fig. 22). The cases shown all have 3.64 wt% UO_2 enrichment.

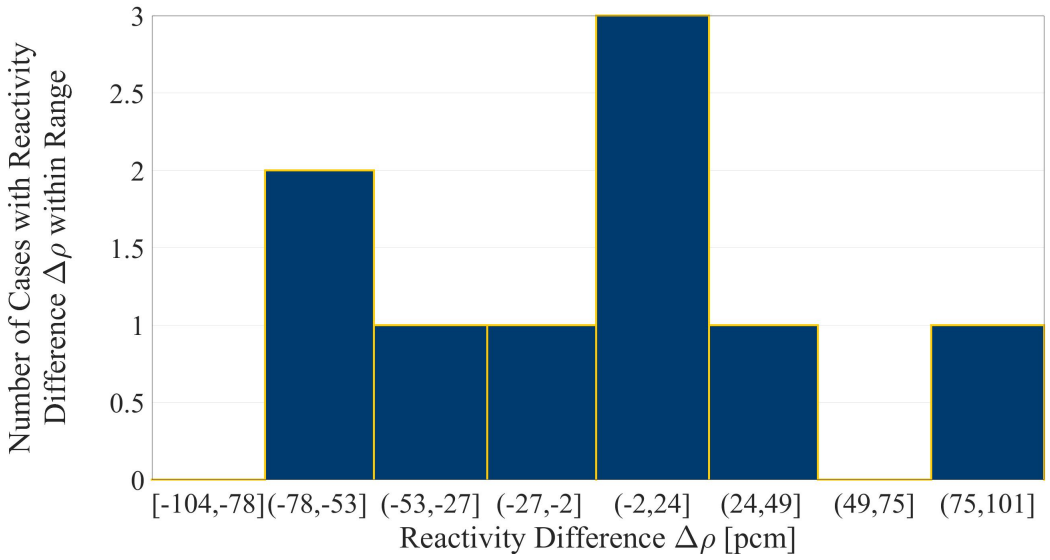

Figure 21. Histogram of reactivity differences for 3.64 wt% UO_2 "fine" single fuel pin cases.

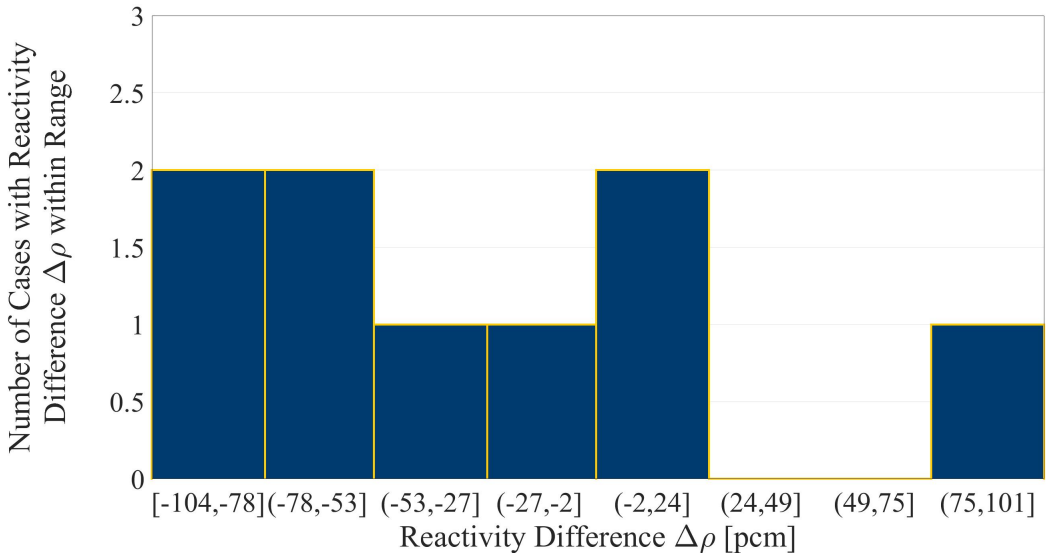

Figure 22. Histogram of reactivity differences for 3.64 wt% UO_2 single fuel pin cases using default parameters.

In comparing the two figures, it is clear that most reactivities predicted by MPACT when using the fine parameters are lower than the reactivities reported by McCARD. Additionally, when using fine parameters, the reactivities are generally closer to the McCARD reference than when default parameters are used. However, the fine solution requires significantly more computational resources to compute; it takes three times as long and uses almost four times as much memory. Given that the average reactivity agreement only improves by 10 pcm when using the finest parameters instead of default values and the tradeoff between accuracy and computational resources, the default parameters obtain suitable k_{inf} values.

4.1.3 Spatial mesh parametric studies

For the spatial mesh studies, the number of radial subdivisions in the innermost region of the fuel cells was changed to be 1, 2, 4, or 5. For reference, the default solution has 3 subdivisions. The cases examined all had 3.64 wt% UO_2. When changing the mesh, ray spacing was set as 0.01 cm, and the azimuthal and polar angles per octant were left at the default values of 16 and 2, respectively. The average differences and standard deviation between the k_{inf} generated using 1, 2, 4, and 5 rings and the k_{inf} calculated by McCARD are shown in 23.

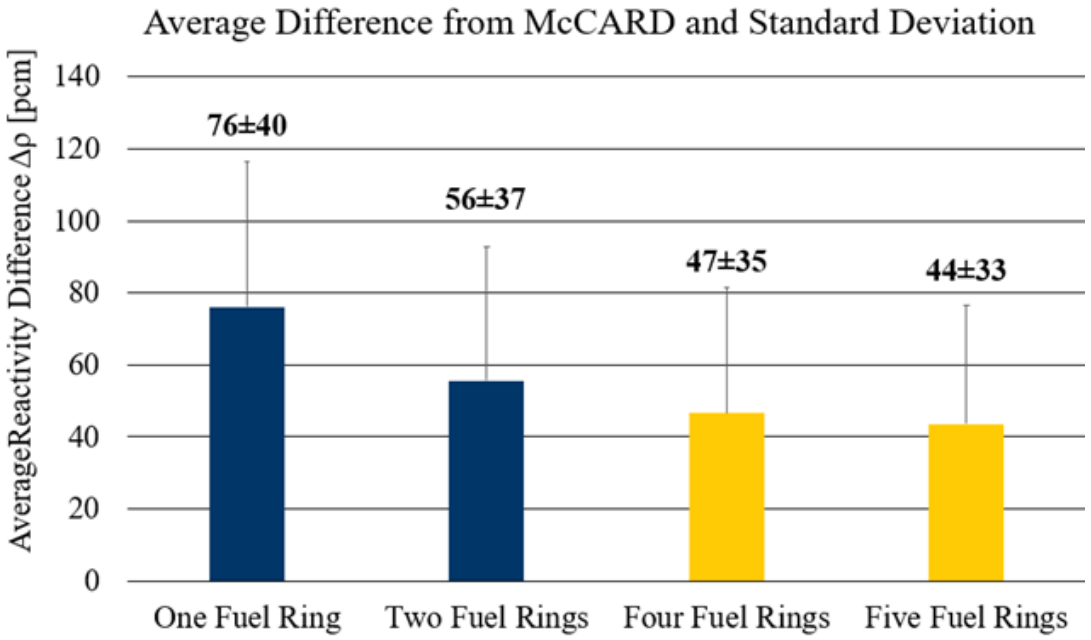

Figure 23. Average difference from McCARD k_{inf} and standard deviation for single pin spatial mesh studies.

In Fig. 23, blue bars indicate parameters that are less fine than the default values, and maize bars indicate parameters that are finer than the default. Using coarser spatial meshes than the default results in reactivity differences from McCARD of 56 pcm for two fuel rings to 76 pcm for one fuel ring. A finer mesh results in reactivity differences from 47 pcm for four fuel rings to 44 pcm for five fuel rings. The reactivity differences for the finer meshes are only 1 pcm to 4 pcm below the reactivity difference of 48 pcm for the default mesh values. Considering that the finer cases take about 1.6 times longer and require about 1.4 times as much memory, and the minimum reactivity difference with McCARD is only 4 pcm lower than when default values are used, the default values are appropriate. Furthermore, altering the MOC parameters has a more significant impact on accuracy than altering the mesh of the problem.

4.1.4 Moderator mesh parameteric studies

For the moderator mesh studies, the number of radial subdivisions in the moderator was changed to be 2, 3, 4, or 5. For reference, the default solution has 1 subdivision. The cases examined all had 3.64 wt% UO_2. When changing the mesh, ray spacing was set to a fine spacing of 0.005 cm, and the azimuthal and polar angles per octant were set at 32 and 3, respectively. Additionally, the number of fuel rings was increased to 5 from the default of 3. The average differences and standard

deviation between the k_{inf} generated using 2, 3, 4, and 5 rings and the k_{inf} calculated by McCARD are shown in Fig. 24.

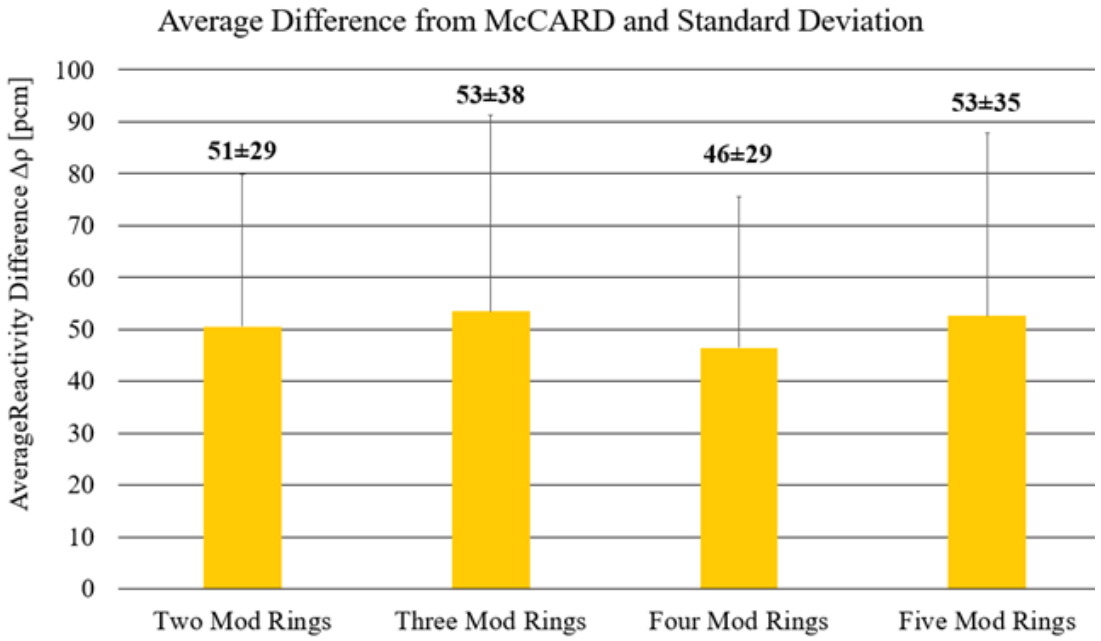

Figure 24. Average difference from McCARD k_{inf} and standard deviation for single pin moderator mesh studies.

When using the default value of one moderator ring, the average reactivity difference between MPACT and McCARD for 3.64 wt% pins is 48 pcm. As Fig. 24 shows, making the mesh finer causes agreement with McCARD to worsen in every case except for four moderator rings. Moreover, the finest moderator mesh of five rings has an average reactivity difference from McCARD of 53 pcm, which is 5 pcm higher than when using default values. Since, as noted earlier, when using the fine mesh, computation time is increased threefold and memory usage is increased fourfold, it was determined that the default value of one moderator ring is most appropriate for use in generating benchmark results.

4.2 Single 2-D Assembly

4.2.1 Benchmark problem results

Each of the nine assembly types (A0, B0, B1, B2, B3, C0, C1, C2, C3) was run using all nine temperature and boron conditions. Fig. 25 is a histogram that shows the number of cases falling each reactivity difference range defined on the horizontal axis.

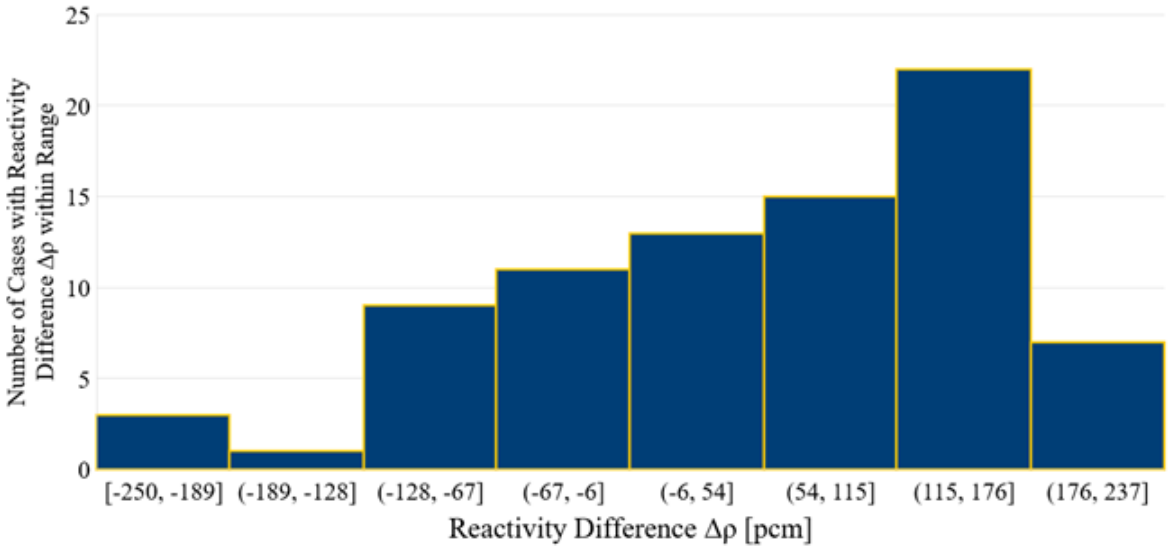

Figure 25. Histogram of reactivity difference for single 2-D assembly problems.

The average difference from the McCARD k_{inf} values was 99 pcm ± 62 pcm, which again can be explained by MPACT using the multigroup approximation for its cross sections. Unlike in the single pin problems, no significant biases in the cross-section libraries resulted in over- or under-predicting; MPACT overestimated k_{inf} in approximately half of the cases and underestimated in the rest compared to McCARD.

The pin powers within the assemblies generated by MPACT are very similar to the McCARD reference solutions, with an overall average RMS pin power difference of 0.22%. Given that a %RMS under 1% is usually satisfactory, the low %RMS difference suggests that MPACT's pin-resolved solution is very effective in generating results in these problems, and that the large guide tubes do not significantly impact the code's accuracy The %RMS pin power differences for each case are depicted in Fig. 26 alongside a list of the ordering of the case conditions within each assembly.

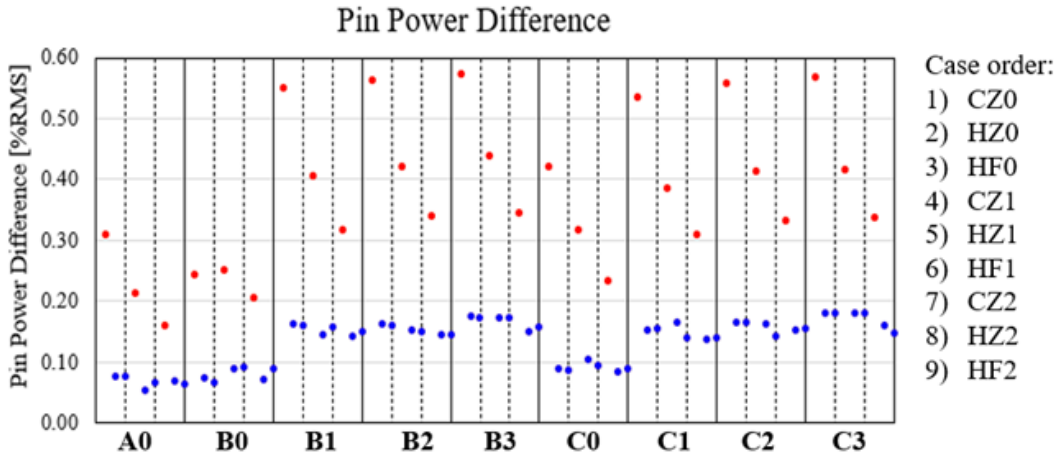

Figure 26. %RMS pin power differences for each 2-D assembly case and list of the case order within each assembly type.

Fig. 26 indicates that greatest deviation from the reference solutions was observed in all CZ cases, no matter the boron concentration. These cases are marked in red, and the pin power differences are significantly higher than all other cases for that assembly.

Table 3 summarizes the data in Fig. 25 and Fig. 26 and shows the average k_{inf} difference as well as the average %RMS pin power difference from McCARD for each assembly type.

Table 3. Single 2-D assembly results by assembly type

Assembly Type	Average k_{inf} $\Delta\rho$ [pcm]	Max. k_{inf} $\Delta\rho$ [pcm]	RMS Pin Power Diff.[%]	Max. Pin Power Diff. [%]
A0	83 ± 68	234	0.12	0.69
B0	76 ± 67	225	0.13	0.60
B1	100 ± 64	201	0.24	1.09
B2	103 ± 67	218	0.25	1.15
B3	143 ± 64	250	0.26	1.10
C0	71 ± 74	237	0.17	0.90
C1	83 ± 51	151	0.22	1.06
C2	113 ± 52	182	0.25	1.08
C3	117 ± 57	204	0.26	1.10

As mentioned in the previous section, reactivity differences are ideally below 200 pcm. For the 2-D assembly problems, eight cases do not meet this goal, and all but two of these have CZ conditions. As such, MPACT shows good agreement with McCARD. Reference [8] also outlines accuracy goals of less than 1.0% RMS difference and less than 1.5% maximum difference for 2-D assembly pin power distributions. Since the highest RMS pin power difference between MPACT and McCARD is 0.57% and the maximum pin power difference is 1.15%, the pin powers calculated by MPACT show excellent agreement with McCARD.

4.2.2 MOC parametric studies

Nine cases were considered for the 2-D assembly MOC studies: for each of the nine assemblies, MOC parameters were independently changed for the CZ0 case. The results were compared to the McCARD k_{inf}. Just as for the single pin cases, variations included using 4, 8, and 32 azimuthal angles per octant instead of the default 16; 1 and 3 polar angles per octant instead of the default 2; and 0.025 cm, 0.01 cm, and 0.005 cm ray spacing instead of the default 0.05 cm. Fig. 27 summarizes the average differences between the k_{inf} generated using each of these parameters and the k_{inf} generated by McCARD as well as the standard deviation.

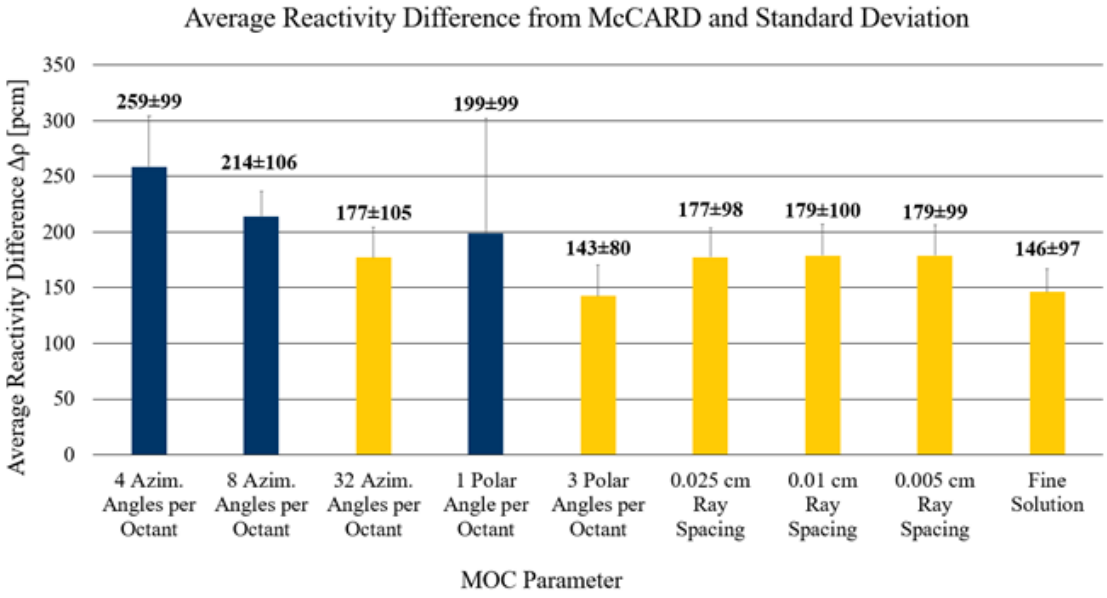

Figure 27. Average difference from MPACT default k_{inf} for 2-D assembly MOC studies.

In Fig. 27, blue bars indicate parameters that are less fine than the default values, and maize bars indicate parameters that are finer than the default. For reference, the average difference from McCARD for 2-D assembly CZ0 cases using default MOC parameters was 133 pcm ± 74 pcm.

Significant disagreement ranging from an average of 199 pcm to 259 pcm exists when parameters are made less fine than the default, thereby indicating that using coarser MOC values worsens agreement with McCARD when compared to the default values, as expected. The maximum absolute difference from McCARD is 371 pcm.

However, when MOC parameters are made finer than the default, the average reactivity difference with McCARD is worse than reactivity difference of 133 pcm when using default parameters in every case; the average difference ranges from 143 pcm to 179 pcm. Even compared to a "fine" solution that had a ray spacing of 0.005 cm, 32 azimuthal angles per octant, and 3 polar angles per octant, the average reactivity difference is 146 pcm, which is 13 pcm higher than the difference when default values are used. A possible explanation is that refining the MOC mesh could be reducing some error cancellation. Specifically, the MPACT cross section library uses super homogenization (SPH) factors to obtain the best possible agreement, even when different calculation methods are used. The SPH factors are determined by comparing pin cell solutions generated using transport corrected P_0 (TCP_0) scattering with solutions generated using continuous energy Monte Carlo

methods. The multigroup resonance integral data is multiplied by these SPH factors. When solving problems using P_2 scattering instead of TCP_0 scattering, as with these benchmark results, the SPH factors become inconsistent, thereby removing some error cancellation and contributing to the significant disagreement observed in Fig. 27 above. Hence, given that every alteration to MOC parameters causes worse agreement with McCARD than for default values, default MOC parameters are most appropriate for use in generating benchmark results.

4.2.3 Spatial mesh parametric studies

For the 2-D assembly mesh study, the number of radial subdivisions in the innermost region of the fuel cells was changed from the default of three rings to be one, two, four, or five rings. The gadolinia mesh was also altered from the default value of ten rings to be one, five, or 15 rings. When varying the mesh, ray spacing was 0.01 cm, and the azimuthal and polar angles per octant were left at the default values. The mesh azimuthal angles were left at the default of 8 per octant. The CZ0 case for each assembly type, the same as was used for the MOC studies, was examined for the spatial mesh studies. The average differences between the k_{inf} generated using the various spatial meshes and the k_{inf} calculated by McCARD as well as the standard deviation are shown in Fig. 28.

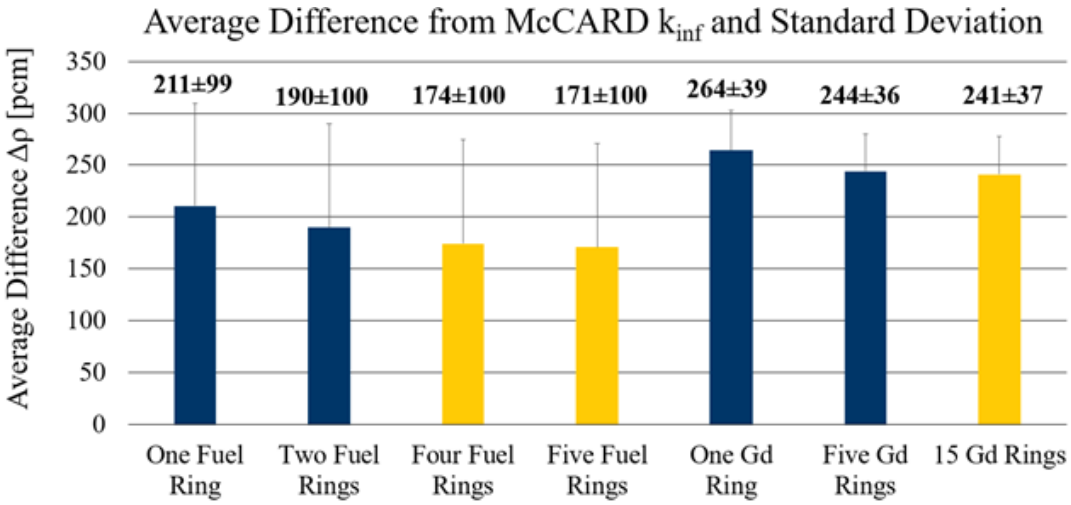

Figure 28. Average difference from MPACT default k_{inf} for 2-D assembly spatial mesh studies.

In Fig. 28, blue bars indicate parameters that are less fine than the default values, and maize bars indicate parameters that are finer than the default. Using coarser spatial meshes than the default results in average reactivity differences from McCARD ranging from 190 pcm to 264 pcm, and using finer spatial meshes results in reactivity differences from 171 pcm to 241 pcm. The maximum absolute difference from McCARD of all of the cases was 331 pcm. Like the MOC parametric studies, every alteration of the spatial mesh, including making it finer, has worse average agreement with McCARD than the default mesh, which has an average reactivity difference from McCARD of 133 pcm. This is again likely due to inconsistencies in the SPH factors due to the use of the P_2 scattering method that are accentuated when the mesh is changed.

Every alteration of the gadolinia mesh results in substantially worse agreement with McCARD than is observed for changing the fuel mesh; the finest gadolinia mesh of 15 rings has an average

reactivity difference of 241 pcm with McCARD, which is 30 pcm worse than the average reactivity difference for the coarsest fuel spatial mesh of one ring.

As with the MOC parametric study, given that every alteration to the fuel and gad meshes causes agreement with McCARD to worsen, it is most optimal to use the default values of three fuel rings and ten gadolinia rings when generating benchmark results.

4.2.4 Comparison of 2-D assembly MPACT "fine" solution to McCARD

To further examine if default parameters generate appropriate benchmark solutions, 2-D assembly results obtained using the "fine" solution, which has a ray spacing of 0.005 cm, 32 azimuthal angles per octant, and 3 polar angles per octant, were compared to McCARD. These solutions were then compared to how close the default solution was to McCARD. All cases considered were CZ0 cases. Table 4 shows the ρ k_{inf} difference and %RMS pin power difference from McCARD for both the solution generated using MPACT's default parameters and the "fine" solution.

Table 4. Comparing default and "fine" solution

Assembly Type	k_{inf} Rho Diff. [pcm]		RMS Pin Power Diff. [%]	
	Default Solution	"Fine" Solution	Default Solution	"Fine" Solution
A0	-76	-56	0.12	0.31
B0	-91	-29	0.12	0.54
B1	-201	-120	0.25	0.50
B2	-218	-220	0.26	0.57
B3	-250	-270	0.27	0.58
C0	-25	-7	0.17	0.42
C1	-106	-167	0.24	0.54
C2	-113	-221	0.26	0.56
C3	-114	-224	0.27	0.57
Average	-133 ± 74	-146 ± 97	0.22	0.51

As seen in Table 4, the average k_{inf} relative difference from McCARD and average RMS pin power differences are both higher for the "fine" solution than using the default parameters. Again, this is likely due to the super homogenization (SPH) factors used by MPACT's cross section library that are determined using TCP_0 scattering. So, when solving problems using P_2 scattering instead of TCP_0 scattering, as with these benchmark results, the SPH factors become inconsistent, thereby removing some error cancellation and contributing to increased disagreement from a more refined mesh. Thus, the default parameters are sufficiently optimized and are appropriate to use to generate benchmark problem results.

Fig. 29 compares pin power differences of the A0 assembly with CZ0 conditions from McCARD for the default and "fine" solution, and clearly indicates that differences in individual pin powers are quite similar for both solutions. Blue represents minimum difference and maize indicates maximum difference from McCARD.

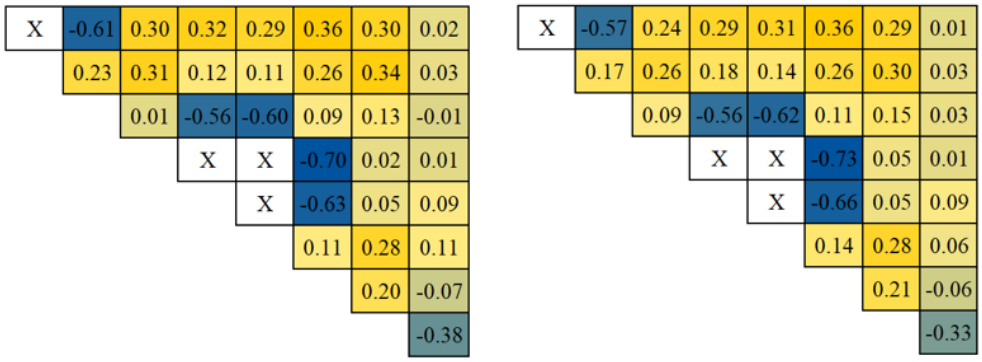

Figure 29. Relative difference [%] in A0 assembly pin powers of MPACT default solution (left) and MPACT "fine" solution (right) from McCARD solution.

4.3 2-D Core

4.3.1 In-out tilt with TCP_0 scattering

MPACT's default scattering method is TCP_0. However, the 2-D core radial power distribution results exhibited significant in-out tilt when the default TCP_0 scattering was used. Fig. 30 shows the radial assembly powers for the HZ1 case when TCP_0 scattering was used.

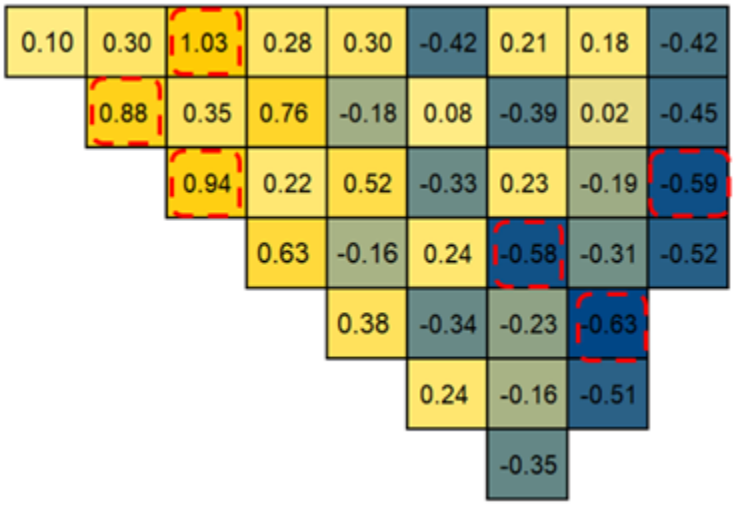

Figure 30. In-out tilt in assembly-wise radial power distribution with default TCP_0 scattering in HZ1 case.

In the figure, maize indicates over-estimation of assembly powers, and blue represents under-estimation. The greatest deviations from McCARD are outlined in red. There are clearly defined regions of over- and under-estimation of assembly powers; maize is concentrated in the center regions, with over-estimation ranging from 0.08% to 1.03%. The periphery is dominated by blue, with under-estimation from -0.16% to -0.63%. For the HF1 case, the RMS assembly power difference was 0.45%, and the maximum difference was 1.03%

To address this in-out tilt, P_2 scattering was used instead. Fig. 31 shows the radial power distribution for the HZ1 case when the P_2 scattering method is used.

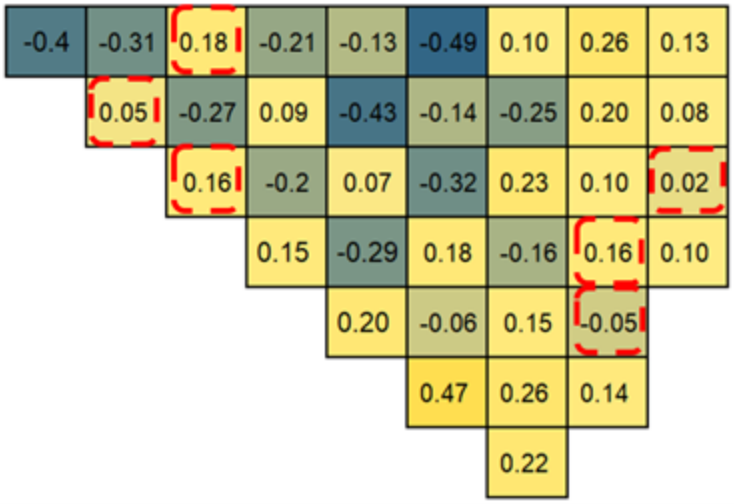

Figure 31. Corrected assembly-wise radial power distribution with P_2 scattering in HZ1 case.

Again, maize represents over-estimation of assembly powers while blue indicates under-estimation. The same color scale is used for Fig. 30 and Fig. 31 to better compare the two. The power distribution is now much more even, and the regions of over- and under-estimation are not so clear. Additionally, the radial assembly powers show much greater agreement with McCARD; The RMS assembly power difference decreased from 0.45% to 0.23%, and the maximum relative power difference decreased from 1.03% to 0.49%.

The HZ1 case is not unique; every case demonstrated substantially improved agreement when P_2 scattering was used. The specific changes to RMS and maximum assembly power differences when changing from TCP_0 to P_2 scattering are outlined in Table 5.

Table 5. Comparing RMS and maximum assembly power differences for TCP_0 and P_2 scattering.

Case Condition	RMS Difference [%]		Max. Difference [%]	
	TCP_0	P_2	TCP_0	P_2
CZ0	1.15	0.41	2.54	0.85
HZ0	0.55	0.34	1.31	0.82
HF0	0.51	0.36	1.13	0.67
CZ1	1.24	0.42	3.10	0.85
HZ1	0.45	0.22	1.03	0.48
HF1	0.84	0.39	1.77	1.02
CZ2	1.92	0.47	4.52	0.87
HZ2	1.05	0.18	2.24	0.40
HF2	1.36	0.21	2.53	0.48
Average	1.01	0.33	2.24	0.72

As shown in Table 5, the average RMS assembly power difference decreased from 1.01% to 0.36% and the average maximum assembly power difference decreased from 2.24% to 0.80% when P_2 scattering was used instead of TCP_0 scattering, clearly indicating the P_2 scattering must be used to

have acceptable agreement with McCARD. Thus, for all benchmark problems, P_2 scattering was used. P_2 scattering was also tested for the single pin and single 2-D assembly problems, and results were significantly different, so those problems were redone using P_2 scattering. The original, TCP_0 results are included in Appendix 1 for reference.

4.3.2 Results generated using P_2 scattering

As outlined above, when P_2 scattering is used, the 2-D core results generated by MPACT demonstrate strong agreement with the McCARD reference solution. Fig. 18 summarizes and compares the 2-D core results generated by McCARD and MPACT for each condition.

Table 6. Summary of 2-D core results and comparison between MPACT and McCARD.

Case Condition	McCARD		MPACT	Comparing MPACT and McCARD		
	k_{eff}	std. [pcm]	k_{eff}	Rho Diff. [pcm]	Assembly Power Diff. RMS [%]	Assembly Power Diff. Max. [%]
CZ0	1.22261	6	1.22040	-148	0.41	0.85
CZ1	1.03687	7	1.03670	47	0.42	0.85
CZ2	0.91050	7	0.91098	182	0.47	0.87
HZ0	1.14693	6	1.14693	0	0.34	0.82
HZ1	1.02305	6	1.02328	72	0.22	0.48
HZ2	0.93015	6	0.93044	131	0.18	0.40
HF0	1.13808	6	1.13768	-31	0.36	0.67
HF1	1.01523	6	1.01512	40	0.39	1.02
HF2	0.92316	6	0.92401	99	0.25	0.64
Average	-	-	-	83 ± 61	0.34	0.73

The rho difference for each condition is below 200 pcm for every case, and the overall average rho difference is 83 pcm ± 61 pcm. The greatest reactivity difference is for the CZ2 case, which overpredicts k-eff by 182 pcm. This maximum difference is below the accuracy goal of 200 pcm difference outlined in [8], indicating good reactivity agreement between MPACT and McCARD.

Regarding the assembly comparisons, MPACT's results agree very well with McCARD; the average RMS assembly power difference is only 0.34%, and the average maximum difference is 0.73%. Reference [8] presents accuracy goals of below 1.5% RMS assembly power differences and below 2.5% maximum assembly power differences. The greatest RMS assembly power difference is 0.47% and the maximum assembly power difference is 1.02%, indicating that MPACT shows good agreement with the power distributions calculated by McCARD.

Generally, the CZ cases have worse reactivity agreement with McCARD than other case conditions. There are several possible explanations for this. Specifically, it is possible that the hydrogen scattering matrix used by either McCARD or MPACT is incorrect; temperature dependence is not accounted for in the scattering kernel for hydrogen, which results in inaccuracies in the scattering matrix. Since hydrogen plays such an important role in light water reactors, small changes in the scattering kernel can substantially impact results [9]. To determine if the scattering matrix used by McCARD caused these issues, single fuel pin and 2-D assembly results generated by MPACT using CZ conditions were compared to those generated by the Monte Carlo code Serpent [10].

The disagreement in pin power and reactivity between MPACT and Serpent was comparable to the disagreement between MPACT and McCARD, indicating that if the cold zero bias is caused by an incorrect scattering matrix, it is the scattering matrix used by MPACT and not McCARD. It was also suggested that there may be a spatial discretization error in which there are too few rings in the mesh for the moderator. However, this was investigated, and refining the moderator mesh did not resolve the cold zero bias.

4.4 3-D Core

4.4.1 3-D core results

Table 7 summarizes and compares the 3-D core results from McCARD and MPACT for each condition. The standard deviation for all Monte Carlo cases is 4 pcm.

Table 7. Summary of 3-D core results and comparison between MPACT and McCARD.

Case Condition	McCARD	MPACT	Comparing MPACT and McCARD				
	k_{eff}	k_{eff}	$\Delta\rho$ [pcm]	Assembly Power Diff.		Axial Power Diff.	
				RMS [%]	Max [%]	RMS [%]	Max [%]
CZ0	1.21765	1.21534	-156	0.46	1.07	0.55	1.95
CZ1	1.03406	1.03448	39	0.46	0.98	1.65	3.04
CZ2	0.90907	0.91046	168	1.17	2.57	0.77	1.39
HZ0	1.13942	1.13938	-3	0.48	1.27	1.38	2.53
HZ1	1.01760	1.01829	67	0.38	0.79	0.88	1.65
HZ2	0.92594	0.92709	134	0.22	0.57	0.34	0.93
HF0	1.13061	1.13013	-38	0.56	1.26	1.18	2.81
HF1	1.00973	1.01013	39	0.32	0.72	0.58	1.91
HF2	0.91899	0.91979	94	0.30	1.03	0.77	1.39
Average	-	-	82 ± 59	0.49	1.14	0.90	1.96

Generally, the results agree well with the McCARD reference solution. The k_{eff} difference is below 150 pcm in every case except for CZ0 and HF0, in which case it was -156 pcm and 168 pcm, respectively. All reactivity differences are below 200 pcm, indicating good reactivity agreement between MPACT and McCARD.

Additionally, all RMS assembly power differences are below 0.56% with the exception of the HF0 case, which had an RMS assembly power difference 1.17%, respectively. Axial power differences are slightly larger; the largest RMS axial power difference is 1.65%, and the maximum axial power difference is 3.04%. Reference [8] gives an accuracy goal of 2.0% RMS difference and 3.0% maximum difference for both radial and axial power distributions. The radial RMS and maximum assembly power differences are all below these goals, indicating good agreement of radial power distributions between MPACT and McCARD. Regarding axial power differences, the RMS differences are all below 2.0%, but the maximum difference of 3.04% exceeds the accuracy goal of 3.0%, albeit slightly. However, all other maximum axial power differences are below 3.0%, with most falling below 2.0%, indicating acceptable agreement between the axial powers calculated by MPACT and those found by McCARD.

For each boron concentration, the temperature condition with the greatest overall deviation from McCARD is the CZ case, which is consistent with the results from previous problems. As noted above, this may be caused by an incorrect hydrogen scattering matrix being used by MPACT.

Fig. 32 depicts the RMS axial power differences for each case.

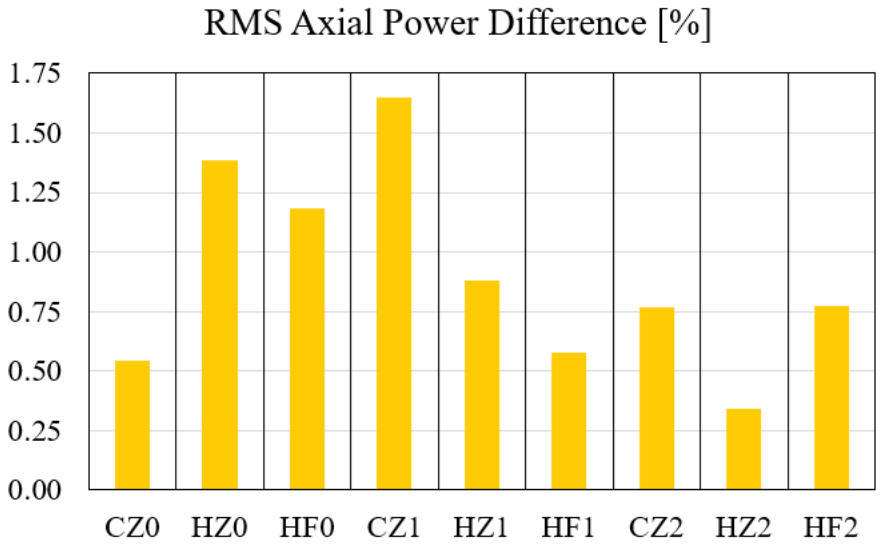

Figure 32. RMS axial power differences for each case condition.

Fig. 32 indicates that generally, axial power agreement increases as boron concentration increases.

Fig. 33 and Fig. 34 show the axial power and relative difference from McCARD for the CZ1 and HZ2 cases, respectively. The axial power and relative difference from McCARD for every case is contained in Appendix 2. The disagreement with McCARD is much greater for the CZ1 case, as indicated by the greater relative difference values, which are represented by the blue line in each figure, in Fig. 33 when compared to Fig. 34.

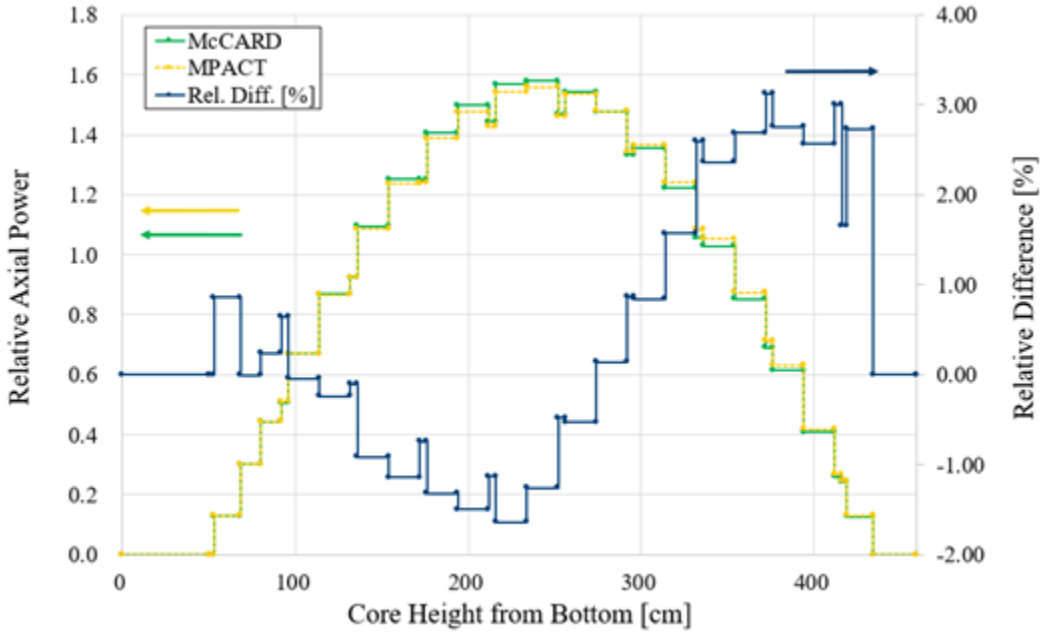

Figure 33. Axial power and relative difference from McCARD for CZ1 case.

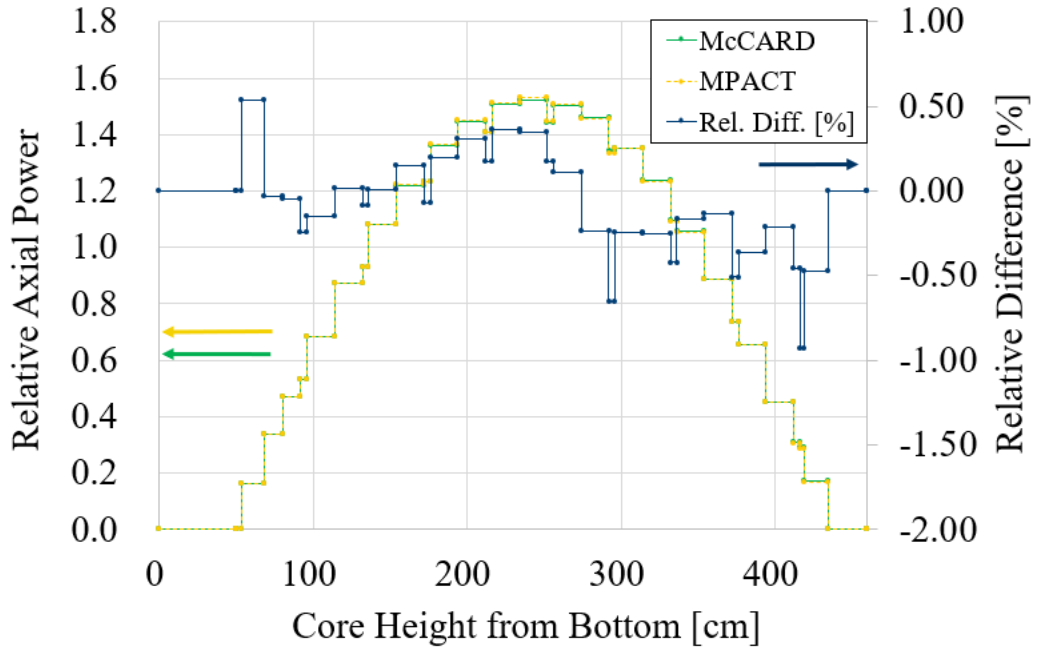

Figure 34. Axial power and relative difference from McCARD for HZ2 case.

4.5 Control Rod Worth

4.5.1 Control rod assembly configuration and problem setup

Fig. 35 shows the control rod assembly configuration for the APR1400. In total, there are seven control rod banks. Five banks are regulating groups, and are labeled 1, 2, 3, 4, and 5, and two banks are shutdown groups labeled A and B. Banks A, B, 1, and some of bank 2 are 12-fingers

assemblies, and some of bank 2 as well as banks 3, 4, and 5 are 4-fingers assemblies.

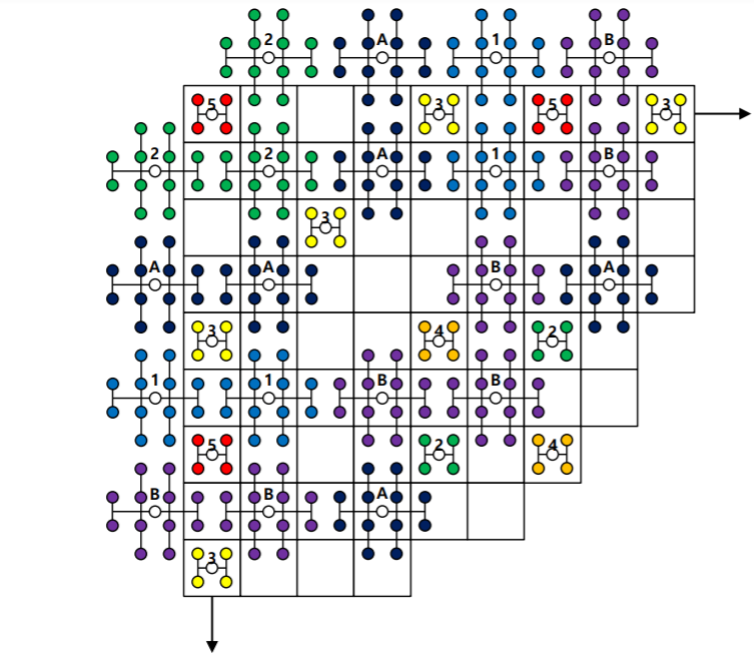

Figure 35. Control rod assembly configuration for APR1400 [2].

All cases used HZ0 conditions. There were seven cases studied for the control rod worth problems, plus the all rods out (ARO) case, which is the HZ0 case from the 3-D core problems. For each case, all seven banks were inserted one at a time, following the order 5 – 4 – 3 – 2 – 1 – B – A. There was no withdrawal of previously considered banks.

4.5.2 Worth equation

The values used to compare results generated by MPACT and McCARD were the accumulated worth and the group worth.

Worth was calculated using Eq. (4)

$$worth = \frac{1}{k_i} - \frac{1}{k_{i-1}} \tag{4}$$

where i is the case index. Since the insertion order follows 5 – 4 – 3 – 2 – 1 – B – A, $i = 0$ corresponds to the ARO case, which has a worth of 0 pcm, $i = 1$ corresponds to just bank 5 inserted, $i = 2$ corresponds to banks 5 and 4 inserted, etc.

4.5.3 Accumulated worth

Accumulated worth is the sum of the worth for all banks inserted thus far and was calculated using the relationship in equation Eq. (5).

$$Accumulatedworth = \sum_{i=1}^{n} (worth_i) \tag{5}$$

where n is the number of inserted banks.

4.5.4 Group worth

Group worth refers to the difference in accumulated worth due to inserting a specific control rod bank and was determined using the formula in Eq. (6).

$$\text{Group worth for case i} = \sum_{i=1}^{n}(worth_i) - \sum_{i=1}^{n-1}(worth_i) \tag{6}$$

For example, Group 2 worth = $\sum_{i=1}^{4}(worth)_i - \sum_{i=1}^{3}(worth)_i$.

4.5.5 Control rod worth results

Table 8 summarizes the control rod worth results and compares the results from MPACT and McCARD.

Table 8. Summary of control rod worth results and comparison between MPACT and McCARD.

Bank(s) Inserted	McCARD		MPACT		Comparing MPACT and McCARD			
	Group Worth [pcm]	Accum. Worth [pcm]	Group Worth [pcm]	Accum. Worth [pcm]	Group Diff. [%]	Accum. Diff. [%]	Assembly Power Diff.	
							RMS [%]	Max [%]
ARO	0.0	0.0	0.0	0.0	-	-	-	-
5	369.0	369.0	366.7	366.7	-0.6	-0.6	0.21	0.37
5-4	322.7	691.7	323.2	689.9	0.1	-0.3	0.31	0.90
5-4-3	999.4	1691.1	1001.3	1691.2	0.2	0.0	0.37	0.66
5-4-3-2	1041.9	2733.0	1042.7	2733.9	0.1	0.0	0.29	0.67
5-4-3-2-1	2010.0	4743.0	2005.4	4739.3	-0.2	-0.1	0.62	1.44
5-4-3-2-1-B	4142.2	8885.2	4163.1	8902.3	0.5	0.2	0.71	1.86
5-4-3-2-1-B-A	7234.0	16119.2	7203.4	16105.7	-0.4	-0.1	0.35	0.84

Again, there is substantial agreement between MPACT and McCARD. All group and accumulated differences are at or below 0.6%. Reference [11] outlines an accuracy goal of below 5% difference in group and accumulated rod bank worths. Since the maximum difference in group and accumulated worths is only 0.6%, MPACT's control rod worths show excellent agreement with McCARD. The greatest deviations from the group and accumulated control rod worths generated by McCARD occur when banks 5 and B are inserted.

Additionally, there is excellent agreement in the assembly powers; all RMS assembly power differences are below 0.71%, and the maximum difference is 1.86%. Assembly power agreement is significantly worse than for all other cases when banks 1 and B are inserted. Similar results were noted for DeCART, and assembly power differences between nTRACER and McCARD were not reported. When examining the radial power distribution, it appears that the greatest differences are in the center of the core, with agreement much stronger on the periphery. Since more absorbers

have been inserted, power peaks are pushed away and the power shape becomes very complicated, resulting in errors in calculations when using transport codes as opposed to Monte Carlo codes. When these cases are excluded, the RMS assembly power differences are at or below 0.37%, and the maximum difference is only 0.90%.

4.6 3-D Core Hot Full Power Depletion

4.6.1 3-D core depletion results

The depletion was done using a 3-D core model with 100% rated power, a coolant inlet temperature of 563.75 K, and critical boron concentration search at each burnup step. In the input, the axial geometry was adjusted slightly; the height of the upper axial reflector was decreased from 25 cm to 5 cm.

No McCARD reference solution was provided for the 3-D core depletion problem, so MPACT results were compared to results generated by other benchmark participants using DeCART and nTRACER [12]. The result from all three codes are shown in Fig. 36.

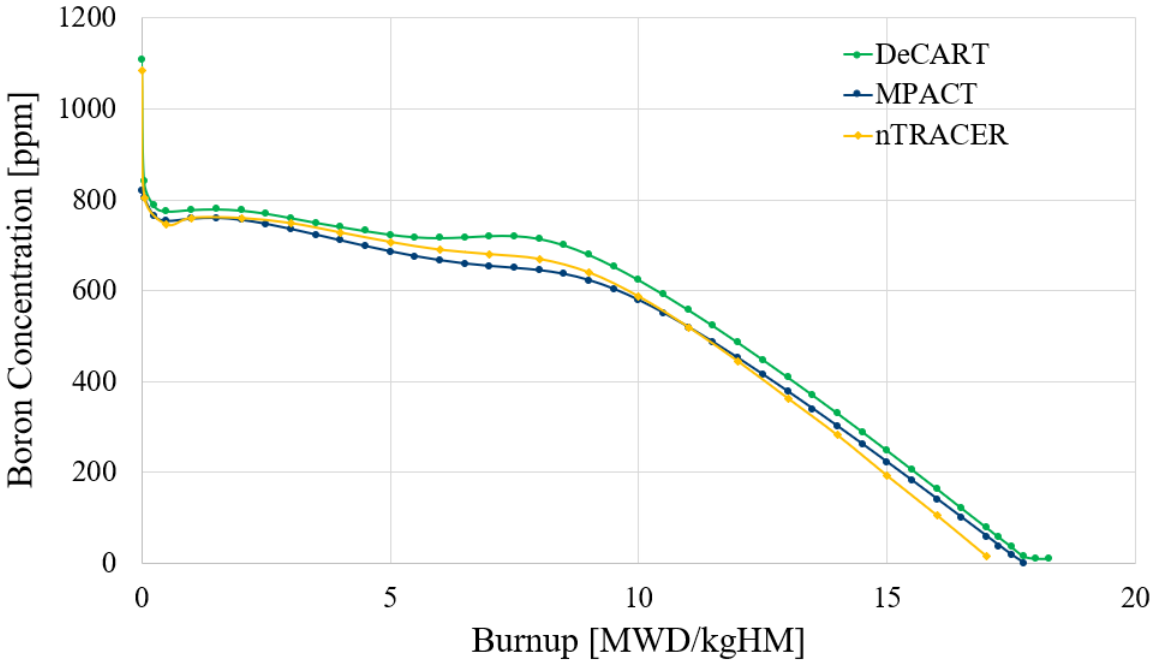

Figure 36. 3-D core depletion results in comparison to solutions generated by other benchmark participants.

Fig. 36 shows that the boron concentration calculated by MPACT reaches 0 ppm by 17.75 MWD/kgHM. Overall, MPACT's results are more similar to nTRACER's than DeCART's. MPACT's boron concentration is almost identical to nTRACER's for burnup of 0.05 MWD/kgHM to 2.5 MWD/kgHM. From 2.5 MWD/kgHM to 10 MWD/kgHM, MPACT reports the lowest boron concentration of the three codes. From 12 MWD/kgHM until the maximum burnup of about 18 MWD/kgHM considered, MPACT's boron concentration is between nTRACER's and DeCART's, but MPACT's boron concentration is closer to DeCART's than nTRACER's from 14.5 MWD/kgHM to 18 MWD/kgHM. For each burnup level, the boron concentration calculated by MPACT is lower

than that calculated by DeCART. Table 9 provides more detail about the different boron concentrations by presenting the boron concentrations calculated by MPACT, DeCART, and nTRACER for different burnups and the difference of DeCART and nTRACER from MPACT.

Table 9. MPACT, DeCART, and nTRACER boron concentrations for different burnups.

Burnup [MWD/kgHM]	MPACT	DeCART		nTracer	
	Boron Concentration [ppm]	Boron Concentration [ppm]	Difference from MPACT	Boron Concentration [ppm]	Difference from MPACT
0	1083.50	1107.56	-24.06	1085.05	-1.55
0.05	804.13	840.73	-36.60	804.85	-0.72
0.5	753.12	774.49	-21.37	745.33	7.79
1	758.04	777.70	-19.66	760.32	-2.28
2	755.54	776.44	-20.90	759.79	-4.25
3	735.58	759.99	-24.41	748.58	-13.00
4	710.47	740.27	-29.80	727.85	-17.38
5	686.32	723.33	-37.01	707.17	-20.85
6	666.70	715.86	-49.17	690.03	-23.33
7	654.05	720.33	-66.28	680.34	-26.29
8	644.79	714.19	-69.40	669.75	-24.96
9	622.80	679.05	-56.25	639.88	-17.08
10	579.05	623.64	-44.59	586.93	-7.88
11	519.56	557.81	-38.25	519.66	0.10
12	451.16	485.78	-34.62	444.04	7.12
13	377.69	409.59	-31.60	362.94	14.75
14	301.01	330.27	-29.26	281.73	19.28
15	221.85	248.19	-26.34	192.45	29.40
16	140.83	164.13	-23.30	105.68	35.15
17	58.76	78.57	-19.81	15.43	43.33
18	0.00	10.00	-10.00	0.00	0.00
Average	-	-	34 ± 16	-	15 ± 20

The average boron concentration difference from MPACT is only 15 ppm for nTRACER and 32 pcm for , indicating that MPACT's calculations are slightly closer to nTRACER's, as noted above. The largest differences from MPACT for occur at 8 MWD/kgHM, this appears to be around the time that the gadolinia is burning out. The prediction of the burnout of gadolinium is well understood to be challenging, so the peak difference being here is not surprising. Additional investigations should be performed to try to identify and confirm the root cause of the peak difference here. For MPACT and nTRACER, the largest difference occurs near the end of cycle. When comparing the two critical boron concentration curves in Fig. 36, it appears that the rate of fuel consumption is different between the two codes, as indicated by the differing slopes after 10 MWD/kgHM. This suggests the κ values, or energy release per fission used for flux normalization in depletion, are different. A suggested follow up study would be to have the 3 codes perform the cycle depletion calculation with the same κ.

4.6.2 Burnup interval sensitivity for Gadolinia

The burnup interval used for the depletion was 14 EFPD, which equals approximately 0.54 MWD/kgHM. There were concerns that this interval may be too large because gadolinia has a large absorption cross section, so the reaction rate of gadolinia changes dramatically over time. As such, a smaller interval may be necessary to obtain accurate results. To test this, burnup intervals of 0.5 MWD/kgHM and 0.25 MWD/kgHM burnup interval for 2D assembly depletion were tested, and the calculated k_{inf} values were compared. The results are shown in Fig. 37.

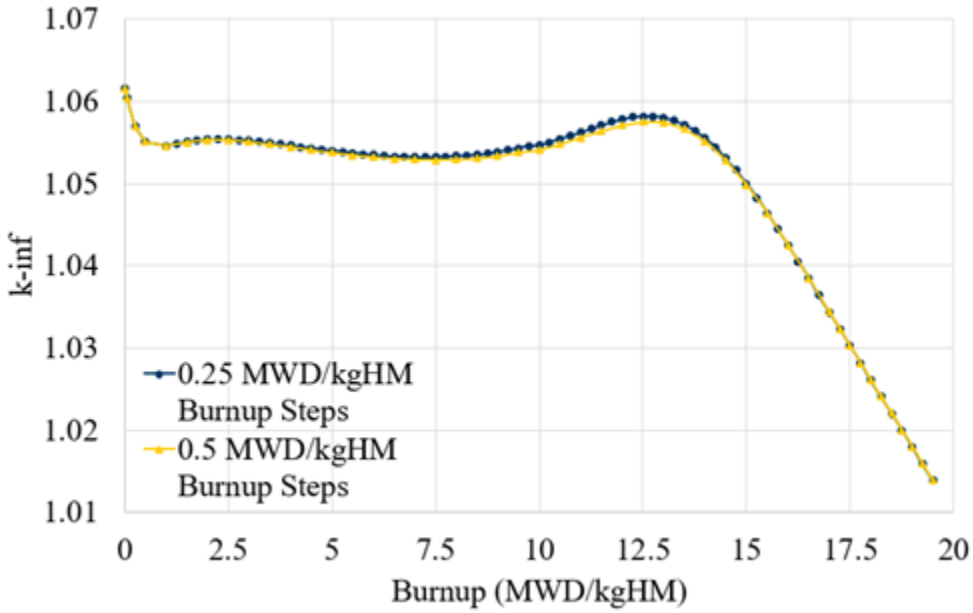

Figure 37. k_{inf} calculated using burnup intervals of 0.5 MWD/kgHM and 0.25 MWD/kgHM.

In Fig. 37, the k_{inf} calculated using the different burnup steps is nearly indistinguishable for every level of burnup. The average rho difference is 21 pcm, and the maximum rho difference is only 63 pcm. Given the strong agreement between the k_{inf} values calculated using both burnup intervals, it was determined that the burnup interval of 0.54 MWD/kgHM, or 14 EFPD, used for the 3-D core depletion problem was acceptable.

5. CONCLUSIONS

Overall, MPACT shows excellent agreement compared to the Monte Carlo reference solution generated by McCARD. MOC and spatial mesh parametric studies indicate that default meshing parameters and options yield results comparable to finely meshed cases, so default parameters are appropriate for use in generating results for benchmark problems. MPACT effectively predicts reactivity for several problem types and conditions. The highest errors exist for CZ conditions, but excluding these cases, the rho reactivity difference is consistently below 100 pcm. Additionally, for the single fuel pin problems, the greatest disagreement existed for the lowest fuel enrichment of 1.71 wt% UO_2, indicating possible enrichment bias in MPACT's cross section library. Moreover, there is strong agreement of the radial and axial power distributions. The use of P_2 scattering corrected the in-out radial power tilt caused by using the default TCP_0 scattering method. With P_2

scattering, all RMS pin and assembly power are differences below 1%, and all RMS axial power differences are below 1.65%. These results are comparable to previous results from the VERA progression problems benchmark [13] [14] and below the accuracy goals outlined in [8] and [11]. Regarding the hot full power 3-D core depletion, there was some variation in the critical boron concentration calculated by MPACT compared to nTracer and . MPACT's boron concentration is closer to nTRACER's concentration than 's for each burnup level.

6. FUTURE WORK

The results of this research generate questions that will be investigated in future work. Specifically, for the single fuel pin studies, there is greater agreement for pin cells with higher fuel enrichments, so this enrichment bias, which may be due to bias in MPACT's cross section library, will be investigated. Also, for each problem, the highest errors existed for cases with cold zero power conditions. This can possibly be explained by an incorrect hydrogen scattering matrix used by MPACT. This possibility will be investigated further. Finally, there were significant differences between MPACT, nTRACER, and in the hot full power 3-D depletion problem. The causes of these differences will be investigated.

7. APPENDIX 1: TCP_0 RESULTS

7.1 Single Fuel Pin Benchmark Problem Results

For the single pin problems, each of the five enrichments (1.71 wt% UO_2, 2.00 wt% UO_2, 2.64 wt% UO_2, 3.14 wt% UO_2, and 3.64 wt% UO_2) was modeled for each of the nine temperature and boron conditions, for a total of 45 cases studied. Fig. 38 is a histogram depicting the number of cases that fall in each reactivity difference range defined on the horizontal axis when TCP_0 scattering is used.

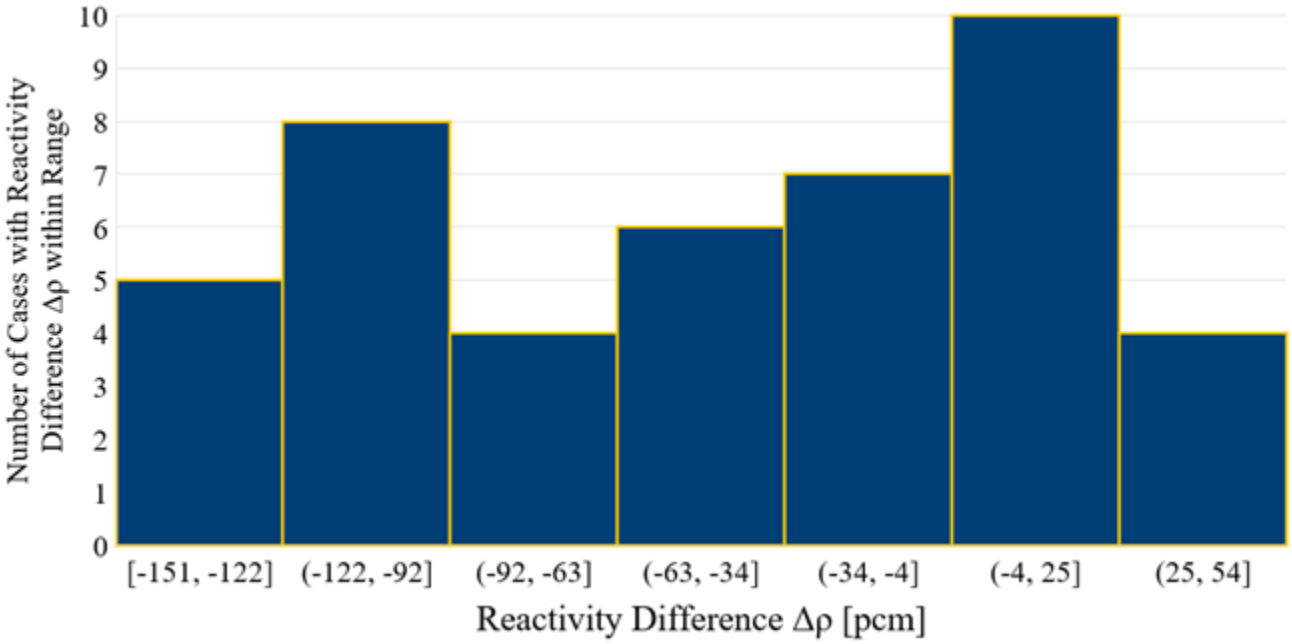

Figure 38. Histogram of reactivity differences for single fuel pin cases when TCP_0 scattering is used.

MPACT and McCARD generally agree very well when TCP_0 scattering is used; the average difference in k_{inf} between the two solutions was 54 pcm ± 46 pcm, which is lower than the average reactivity difference of 63 pcm ± 44 pcm when P_2 scattering is used. As before, this difference can be attributed to MPACT's usage of a multigroup approximation as opposed to McCARD's continuous energy cross section representation. Similarly to when P_2 scattering is used, in 31 of the 45 cases studied, MPACT had a lower k_{inf} than McCARD, demonstrating a possible bias in the cross-section libraries. The maximum difference in k_{inf} was 151 pcm, and the minimum difference was 2 pcm.

Table 10 contains the average reactivity difference, standard deviation, and maximum reactivity difference for various categories of cases to better identify specific trends in the results. The largest relative differences were observed for cases with CZ conditions, possibly due to the aforementioned incorrect hydrogen scattering matrix used by MPACT. Additionally, as observed when P_2 scattering was used, boron concentration had a substantial impact on accuracy, as observed in Table 10, which shows agreement with McCARD improving significantly as boron concentration increases.

Table 10. Average reactivity difference, standard deviation, and maximum difference for various groups of single fuel pin cases when TCP_0 scattering is used.

Condition	Average k_{inf} $\Delta\rho$ [pcm]	Standard Deviation [pcm]	Maximum Difference [pcm]
Overall	54	46	151
0 ppm	110	22	151
1000 ppm	31	25	95
2000 ppm	14	21	34
1.71 wt%	56	69	151
2.00 wt%	45	66	134
2.64 wt%	39	57	122
3.00 wt%	39	52	116
3.64 wt%	34	47	104
CZ	59	55	151
HZ	20	53	104
HF	48	58	138

Every group of single pin problems has an equal or lower reactivity difference or maximum difference when TCP_0 scattering is used compared to when P_2 scattering is used.

7.2 Single 2-D Assembly Benchmark Problem Results

Each of the nine assembly types (A0, B0, B1, B2, B3, C0, C1, C2, C3) was run using all nine temperature and boron conditions as well as TCP_0 scattering. Fig. 39 is a histogram that shows the number of cases falling each reactivity difference range defined on the horizontal axis when TCP_0 scattering is used.

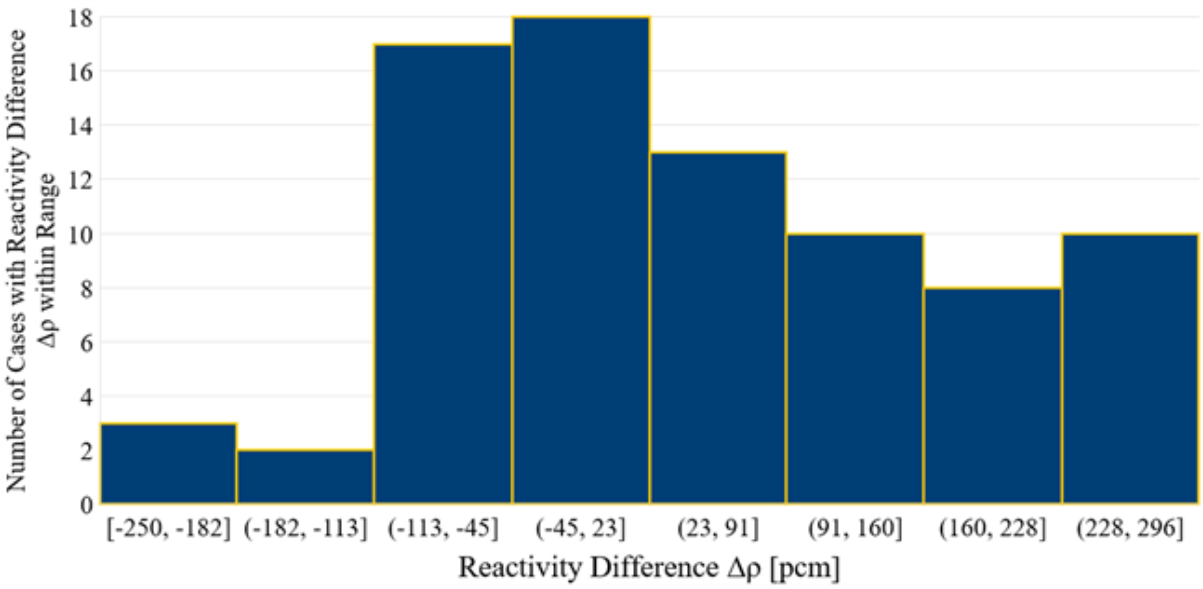

Figure 39. Histogram of reactivity difference for single 2-D assembly problems when TCP_0 scattering is used.

The average difference from the McCARD k_{inf} values was 106 pcm ± 86 pcm, which is higher than the average difference of 99 pcm ± 62 pcm when P_2 scattering is used.

The pin powers within the assemblies generated by MPACT using TCP_0 scattering are very similar to the McCARD reference solutions, with an overall average RMS pin power difference of 0.21%, which is the same as when P_2 scattering is used. Thus, the scattering method impacts reactivity agreement much more than pin power agreement. The %RMS pin power differences for each case are depicted in Fig. 40 alongside a list of the ordering of the case conditions within each assembly.

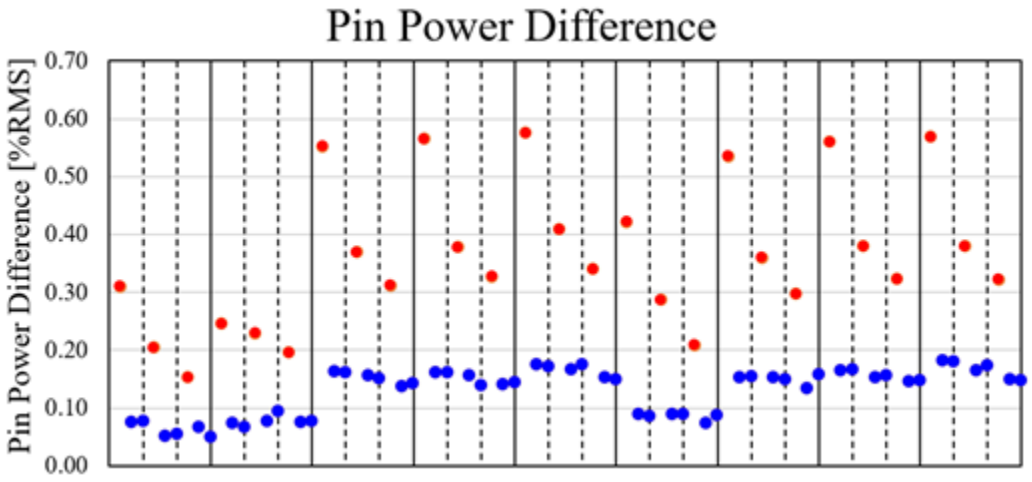

Figure 40. %RMS pin power differences for each 2-D assembly case and list of the case order within each assembly type when TCP_0 scattering is used.

Fig. 40 indicates that greatest deviation from the reference solutions was observed in all CZ cases, no matter the boron concentration, which is the same as when P_2 scattering is used. These cases

are marked in red, and the pin power differences are significantly higher than all other cases for that assembly.

Table 11 summarizes the data in Fig. 39 and Fig. 40 and shows the average k_{inf} difference as well as the average %RMS pin power difference from McCARD for each assembly type.

Table 11. Single 2-D assembly results by assembly type when TCP_0 scattering is used.

Assembly Type	Average k_{inf} $\Delta\rho$ [pcm]	RMS Pin Power Diff. [%]
A0	57 ± 44	0.12
B0	55 ± 32	0.13
B1	114 ± 76	0.24
B2	117 ± 78	0.24
B3	176 ± 109	0.26
C0	65 ± 35	0.16
C1	86 ± 60	0.23
C2	138 ± 96	0.24
C3	143 ± 99	0.25

Overall, compared to when P_2 scattering is used, the results when TCP_0 scattering is used have greater reactivity differences and the same or 0.1% lower RMS pin power differences.

8. APPENDIX 2: ALL 3-D CORE AXIAL POWER GRAPHS

Fig. 41 through Fig. 49 are graphs showing the axial power and agreement with McCARD for all 3-D core cases.

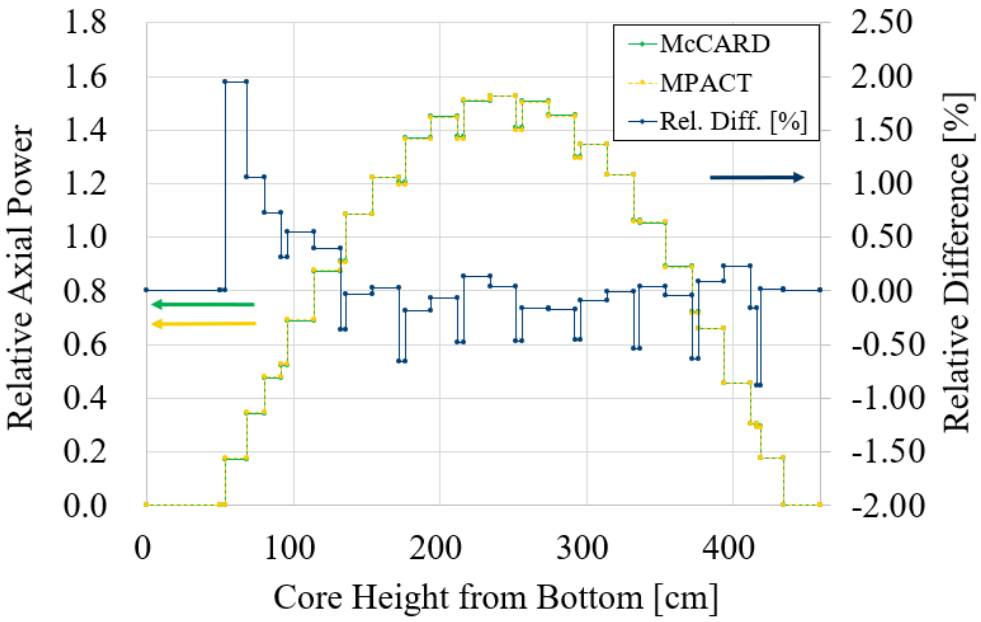

Figure 41. Axial power and relative difference from McCARD for CZ0 case.

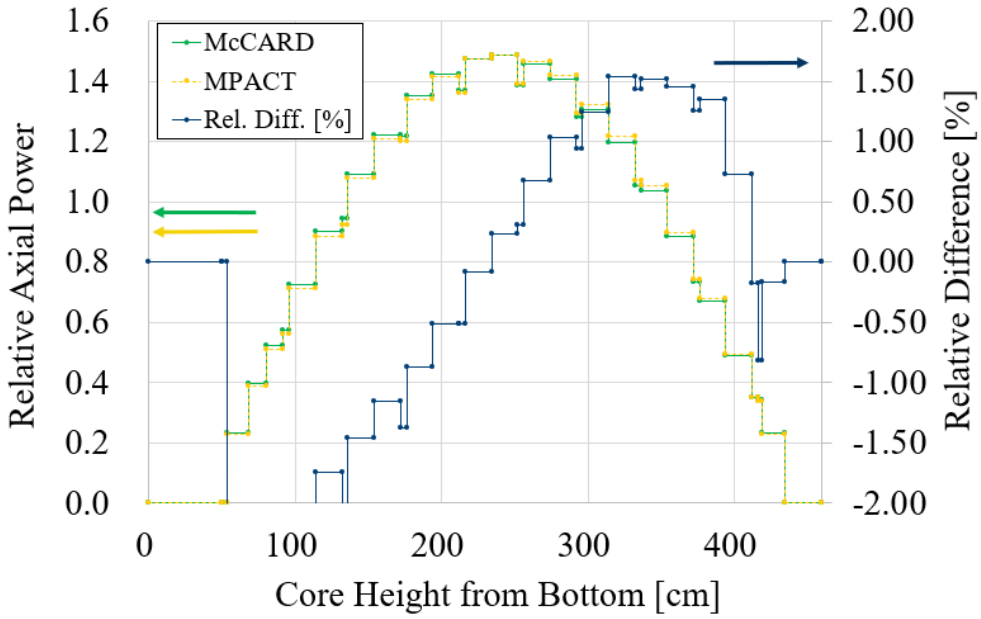

Figure 42. Axial power and relative difference from McCARD for HZ0 case.

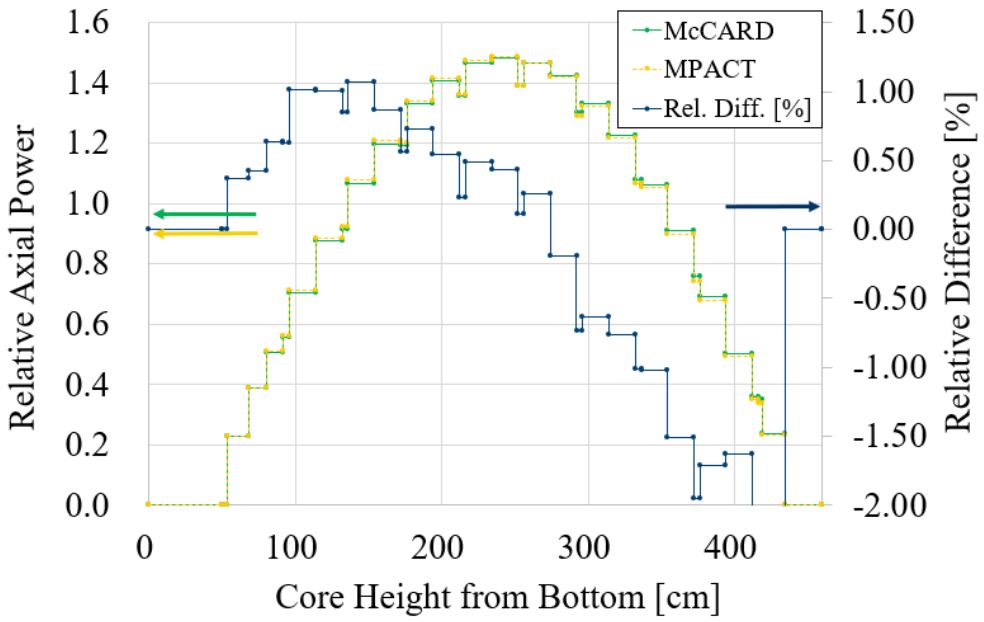

Figure 43. Axial power and relative difference from McCARD for HF0 case.

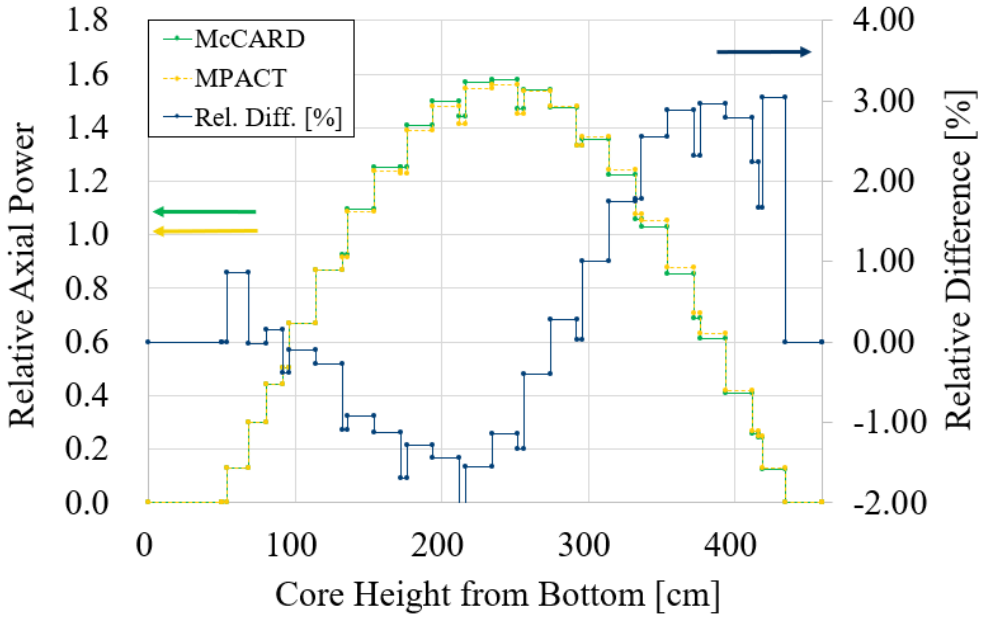

Figure 44. Axial power and relative difference from McCARD for CZ1 case.

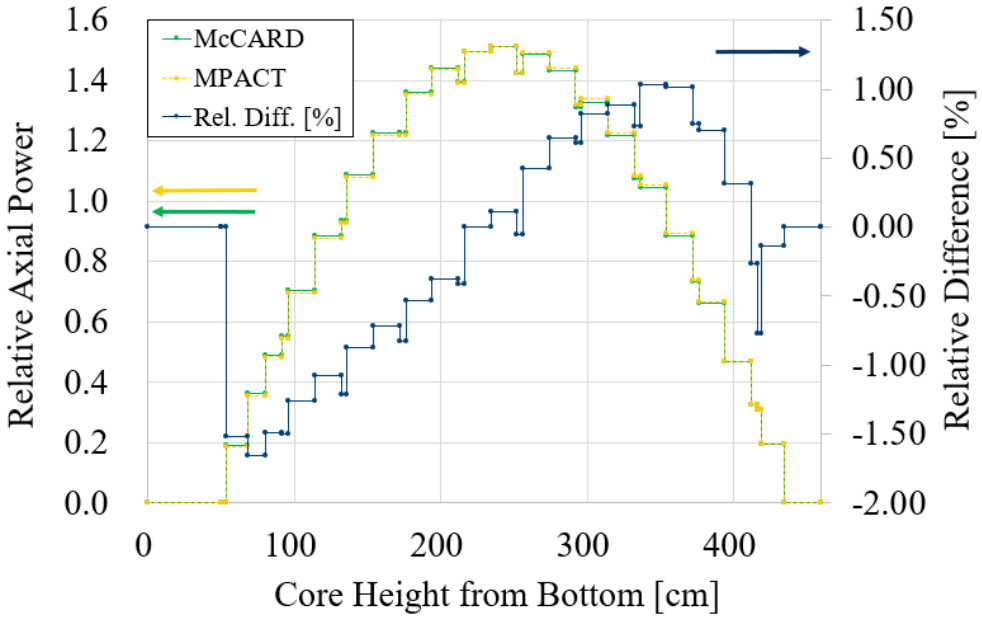

Figure 45. Axial power and relative difference from McCARD for HZ1 case.

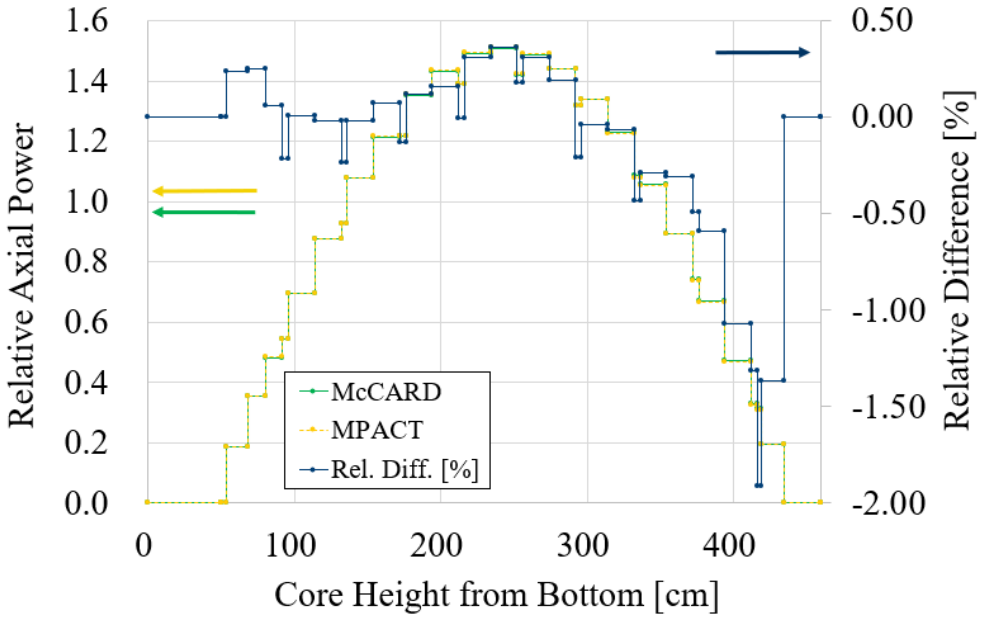

Figure 46. Axial power and relative difference from McCARD for HF1 case.

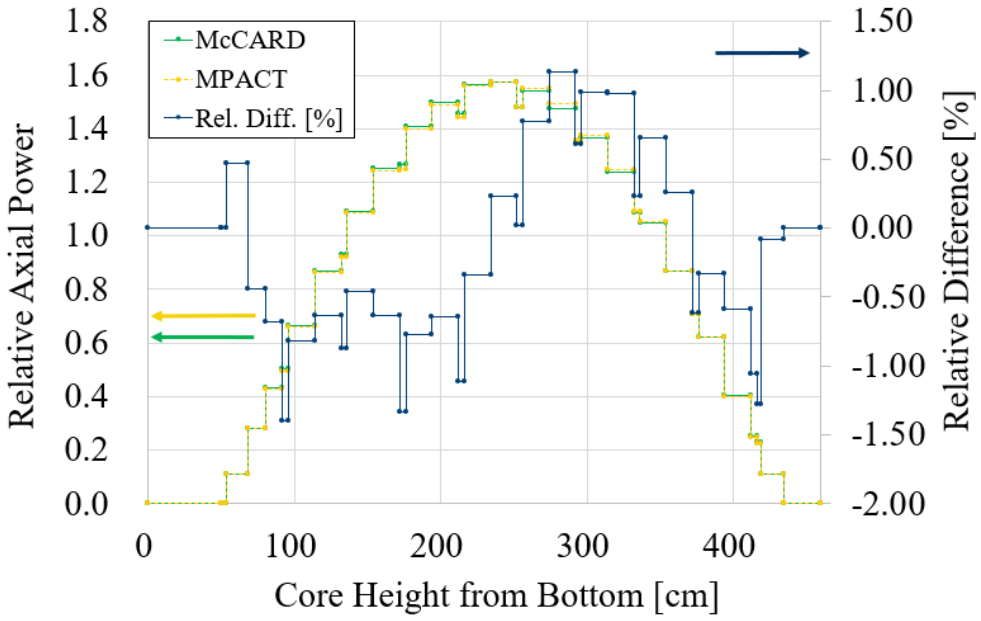

Figure 47. Axial power and relative difference from McCARD for CZ2 case.

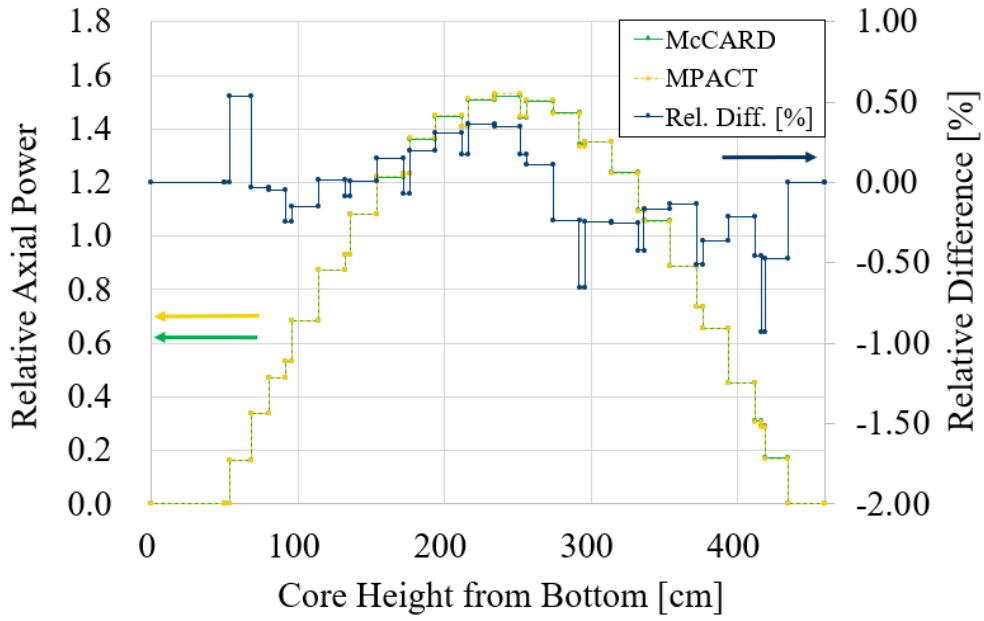

Figure 48. Axial power and relative difference from McCARD for HZ2 case.

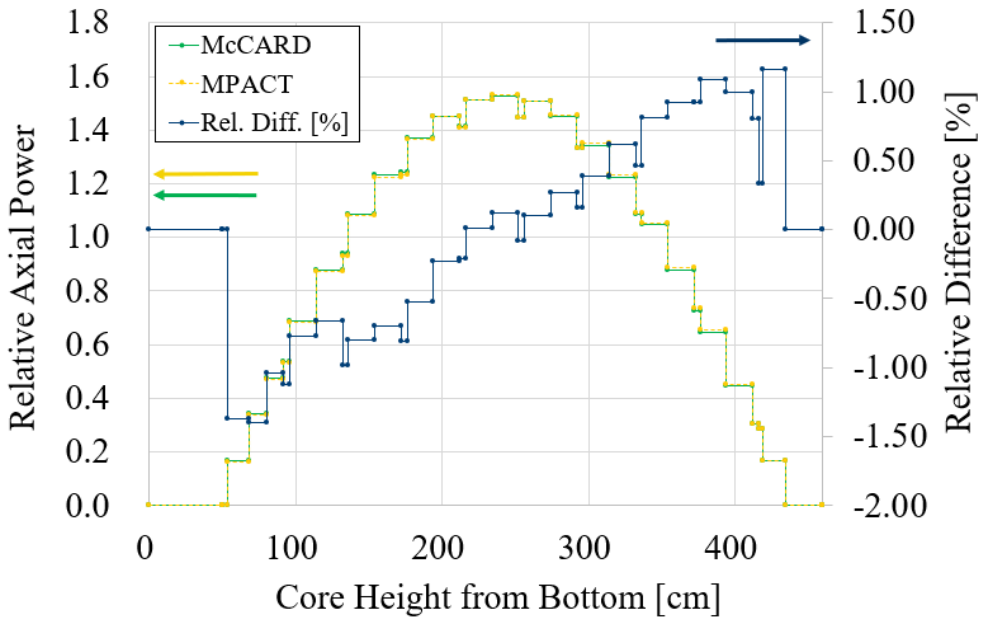

Figure 49. Axial power and relative difference from McCARD for HF2 case.

ACKNOWLEDGEMENTS

This work was performed under the I-NERI in collaboration with Oak Ridge National Laboratory (ORNL), Argonne National Laboratory (ANL), NC State University, KAERI, Seoul National University and Ulsan National Institute of Science and Technology. It was supported by the Consortium for the Advanced Simulation of Light Water Reactors (CASL), an Energy Innovation Hub for Modeling and Simulation of Nuclear Reactors under U.S. Department of Energy Contract No. DE-AC05-00OR22725. This research also made use of the resources at the High Performance Computing Center at Idaho National Laboratory, that is also supported by the Office of Nuclear Energy of the U.S.Department of Energy and the Nuclear Science User Facilities under Contract No. DE-AC07-05ID14517. The authors also wish to express their personal gratitude to Dr. Jin-Young Cho, Prof. Han-gyu Joo, Dr. Seungsu Yuk, and Junsu Kang for their helpful contributions in the analysis of this benchmark.

REFERENCES

[1] "Fiscal Year 2013 Annual Report." Technical Report I-NERI-2013, U.S. Department of Energy Office for Nuclear Energy (2013).

[2] S. Yuk. "APR1400 Reactor Core Benchmark Problem Book." Technical Report RPL-INERI-CA-004, Korea Atomic Energy Research Institute, Daejeon, South Korea (2019).

[3] H. J. Shim, B. S. Han, J. S. Jung, H. J. Park, and C. H. Kim. "McCARD: Monte Carlo Code for Advanced Reactor Design and Analysis." *Nuclear Engineering and Technology*, **volume 44**, pp. 161–176 (2012).

[4] "MPACT Theory Manual Version 2.2.0." Technical Report CASL-U-2016-1107-000, Consortium for Advanced Simulation of Light Water Reactors (2016).

[5] H. G. Joo, J. Y. Cho, K. S. Kim, C. C. Lee, and S. Q. Zee. "Methods and Performance of a Three-Dimensional Whole-Core Transport Code DeCART." In *PHYSOR 2004*, pp. 134–156. Chicago, IL, United States of America (2004).

[6] H. Hong and H. Joo. "Analysis of the APR1400 PWR Initial Core with the nTRACER Direct Whole Core Calculation Code and the McCARD Monte Carlo Code." In *Transaction of the KNS Spring Meeting*. Jeju, Korea (2017).

[7] S. Yuk. "DeCART Solutions of APR1400 Reactor Core Benchmark Problems." Technical Report KAERI/TR-7826/2019, Korea Atomic Energy Research Institute, Daejeon, South Korea (2019).

[8] K. S. Kim, K. T. Clarno, C. Gentry, D. Wiarda, M. L. Williams, B. Kochunas, Y. Liu, S. Palmtag, and A. T. Godfrey. "Development of the V4.2m5 and V5.0m0 Multigroup Cross Section Libraries for MPACT for PWR and BWR." Technical Report CASL-U-2017-1280-000, Oak Ridge National Laboratory ORNL (2017). URL http://www.osti.gov/servlets/purl/1352789/.

[9] H. Park. *Resonance Treatment Innovations for Efficiency and Accuracy Enhancement in Direct Whole Core Calculations of Water-Cooled Power Reactors*. Ph.D. thesis, Seoul National University, Seoul, South Korea (2018).

[10] J. Leppänen, M. Pusa, T. Viitanen, V. Valtavirta, and T. Kaltiaisenaho. "The Serpent Monte Carlo code: Status, development and applications in 2013." *Annals of Nuclear Energy*, **volume 82**, pp. 142–150 (2014).

[11] K. Smith and B. Forget. "Challenges in the Development of High-Fidelity LWR Core Neutronics Tools." In *Int. Conf. on Mathematics and Computational Methods Applied to Nuclear Science and Engineering*. Idaho, United States of America (2013).

[12] J. Kang and H. G. Joo. "nTRACER Solutions of APR1400 Benchmark and Fast Reactor Analysis Status." 3rd I-NERI Progress Meeting (2019).

[13] A. T. Godfrey. "MPACT Testing and Benchmarking Results." Technical Report CASL-U-2014-0045-000, Consortium for Advanced Simulation of Light Water Reactors (2014).

[14] T. Downar, B. Kochunas, and B. Collins. "MPACT Verification and Validation Manual (rev

4).” Technical Report CASL-U-2018-1641-000, Consortium for Advanced Simulation of Light Water Reactors (2018).